INVESTIGATION OF POST SEISMIC DEFORMATION IN KARLIOVA (TURKEY) INFERRED FROM INSAR ANALYSIS

by

Koray Horasan

B.S., Geodesy and Photogrammetry Engineering, Yıldız Technical University, 2007

Submitted to Kandilli Observatory and Earthquake Research Institute for
Graduate Studies in Science and Engineering in partial fulfillment of
the requirements for the degree of
Master of Science

Graduate Program in Geodesy

Boğaziçi University

2013

INVESTIGATION OF POST SEISMIC DEFORMATION IN KARLIOVA (TURKEY) INFERRED FROM INSAR ANALYSIS

APPROVED BY:

Assoc. Prof. Dr. Aslı Doğru . . . . . .
(Thesis Supervisor)

Prof. Dr. Haluk Özener . . . . . .

Prof. Dr. Gönül Toz . . . . . .
(Istanbul Technical University)

DATE OF APPROVAL: 07.06.2013

ACKNOWLEDGEMENTS

Firstly, I am sincerely grateful to my thesis supervisor, Assoc. Prof. Dr. Aslı Doğru for her encouragement and moral support throughout preparation of this thesis. I am also thankful to the members of the jury, Prof. Dr. Haluk Özener and Prof. Dr. Gönül Toz for their support and encouragement in the study.

I want to convey special thanks to David Sandwell, Matt Wei and Xiaopeng Tong who spent their invaluable time to answer my questions about GMTSAR. I am also grateful to ERDAS for providing ERDAS IMAGINE software, especially Volkan Pasınlı.

Lastly, I would like to thank my wife, Meram Mısır Horasan and my family for the endless support, patience and understanding along this period. They have always trusted and believed in me. I also wish to thank all my dear friends for their support and understanding during my study.

ABSTRACT

INVESTIGATION OF POST SEISMIC DEFORMATOIN IN KARLIOVA (TURKEY) INFERRED FROM INSAR ANAYSIS

Interferometric Synthetic Aperture Radar is a new technique used in investigating the deformations occurring on the earth surface. By its capability of providing much broader domain coverage as compared to any other available techniques, geologists are using the interferometric synthetic aperture radar technique in many areas of their research and primarily crustal deformation.

The purpose of this study is to observe the post-seismic impacts using the interferometry technique. In line with this purpose, the effects of deformations resulting from post-seismic impacts of earthquakes have been analyzed with the interferometric synthetic aperture radar technique. The region Karlıova was chosen as the study area. Karlıova-Bingöl-Erzincan triangle is located in the junction of the two most important transform faults: the North Anatolian Fault (NAF) and the East Anatolian Fault (EAF). The area between that two transform faults is a place where KDGB and KB-GD trending cross-fault systems is developed. Therefore, it is the region of the highest concentrations of the active faults in Turkey. The earthquakes that occurred in this region between 2005-2008 were examined in detail.

With this study using the InSAR technique, for two separate earthquakes (10.12.2005 Mw=5.2 Depth:18 km and 26.08.2007 Mw=5.1 Depth:5km), a deformation in the direction of the satellite view of 56 mm during 2005-2006 and 140 mm during 2006-2008 has been determined respectively. In the interferograms generated by using the radar images in the C-band, one fringe theoretically corresponds to a deformation of half the radar wavelength. Therefore, deformations less than 28 mm in the area cannot be determined by the InSAR technique. The SAR data differ from the GPS data in time. During this time range, 17 earthquakes of moderate magnitude have also occurred in the area. The results differ from each other significantly since InSAR measurements contain post-seismic deformation while GPS observations do not. The spatial density of GPS sites is limited. Moreover, noisy interferograms due to atmospheric signal, and phase unwrapping errors affects the accuracy assessment and interpretation of the results.

ÖZET

KARLIOVA BÖLGESİNDE İNSAR TEKNİĞİ İLE DEPREM SONRASI OLUŞAN DEFORMASYONLARIN ARAŞTIRILMASI

Son yıllarda interferometrik yapay açıklı radar tekniği, yeryüzünde meydana gelen deformasyonların incelenmesinde yeni bir araç olarak kullanılmaktadır. Yer bilimcileri interferometrik yapay açıklı radarın diğer ölçme yöntemleriyle karşılaştırılmayacak düzeyde geniş bir çalışma alanı sağlamasından dolayı tekniği başta kabuk deformasyonu olmak üzere birçok farklı alanda kullanmaktadırlar.

Bu çalışmanın amacı interferometri tekniği kullanılarak, deprem sonrası oluşan etkileri gözlemlemektir. Bu amaç doğrultusunda interferometrik yapay açıklıklı radar tekniği ile, deprem sonrası oluşan deformasyon etkileri gözlemlenmiştir. Çalışma alanı olarak Karlıova Bölgesi seçilmiştir. Erzincan-Karlıova-Bingöl üçgeni Türkiye'nin en önemli iki transform fayı olan Kuzey Anadolu Fayı (KAF) ile Doğu Anadolu Fayı (DAF)'nın birleşme bölgesinde yer alır. İki transform fay arasındaki bölgede; KDGB ve KB-GD uzanımlı çapraz fay sistemlerinin gelişmiş olduğu bu alan Türkiye'de aktif fay yoğunluğunun en fazla olduğu bir bölgedir. Bölgede 2005-2008 yılları arasında meydana gelen depremler incelenmiştir.

Bu çalışma ile InSAR tekniği kullanılarak iki ayrı deprem (10.12.2005 Mw=5.2 Derinlik:18 km and 26.08.2007 Mw=5.1 Derinlik:5km) için uydu bakış doğrultusunda sırası ile 2005-2006 arası için 56 mm, 2006-2008 arası için 140 mm deformasyon tespit edilmiştir. C-bandındaki radar görüntüleri kullanılarak oluşturulan interferogramlarda teorik olarak 1 örge, radar dalga boyunun yarısı kadar deformasyona karşılık gelmektedir. Dolayısıyla, bölgede 28 mm'den daha küçük deformasyonlar İnSAR tekniği ile tespit edilememektedir. SAR verileri zamansal olarak GPS verilerinden farklılık göstermektedir. Bu zaman aralığında da orta büyüklükte 17 adet deprem meydana gelmiştir. Bu farkın nedeni, deprem sonrası hareketin InSAR ölçülerinin içerisinde olması, GPS ölçüleri içerisinde olmaması ve depremin etkisinin görüldüğü lokasyonda GPS istasyonunun bulunmayışı olarak değerlendirilmektedir.

TABLE OF CONTENTS

LIST OF FIGURES

LIST OF TABLES

LIST OF SYMBOLS

λ	Wavelength
R	Distance
Ha	Altitude of ambiguity
B	Baseline
Φ	Phase
$\Delta\Phi_{int}$	Interferometric phase
Φ_{topo}	Topographic phase
γ	Viewpoint angle
μ	Velocity of object
Θ	Phase difference
Φ	Azimuth
η	Reflection angle
W_G	Swath width
R	Slant range
B_R	Band width
R_G	Range resolution
W_A	Length of antenna
f_{Do}	Doppler frequency
Vst	Relative velocity
δx	Azimuth resolution

LIST OF ACRONYMS / ABBREVIATIONS

USGS	United States Geological Survey
GPS	Global Positioning System
SAR	Synthetic Aperture Radar
InSAR	Interferometric Synthetic Aperture Radar
DInSAR	Differential Interferometric Synthetic Aperture Radar
AN	Anatolian Plate
AE	Aegean Plate
Ma	Million Years
M	Magnitude
KOERI	Kandilli Observatory and Earthquake Research Institute
NEMC	National Earthquake Monitoring Center
GDMRE	General Directorate of Mineral Research and Exploration
ALOS	Advanced Land Observation Satellite
ASAR	Advanced Synthetic Aperture Radar
ATSR	Along Track Scanning Radiometer
DEM	Digital Elevation Model
DESCW	Display Earth Remote Sensing Swath Coverage of Windows
DORIS	Delft Institute of Earth Observation and Space Systems
ENVISAT	European Environment Satellite

ERS	European Remote Sensing
ERS-1	European Remote Sensing-1
ERS-2	European Remote Sensing-2
ESA	European Space Agency
LLR	Lunar Laser Ranging
JERS-1	Japanese Earth Resourse Satellite-1
KOERI	Kandilli Obsevatory and Earthquake Research Institute
MWR	Microwave Radiometer
MERIS	Medium Resolution Imaging Spectrometer
NASA	National Aeronautics and Space Administration
NEMC	National Earthquake Monitoring Center
PALSAR	Phased Array Type L-band Synthetic Aperture Radar
PRT	Pulse Repetition Time
PSInSAR	Permanent Scattered Interferometric Synthetic Aperture Radar
RA	Radar Altimeter
RADARSAT	Radio Detection and Ranging Satellite
SIR	Shuttle Imagining Radar C
SLAR	Side Looking Airborne Radar
SLC	Single Look Complex
SLR	Satellite Laser Ranging
VLBI	Very Long Baseline Interferometry

1. INTRODUCTION

Natural disasters are occurrences that human beings cannot prevent or control. A disaster can be ostensive defined as any tragic event stemming from events such as earthquakes, floods, catastrophic accidents, fires, or explosions. Every year thousands of people die just because of lethal disasters.

In the World, every country is subjected to several disasters which occur according to environmental circumstances. Between these countries, especially Turkey has a great risk because of vulnerable hazards.

According to the UN ISDR database the country has recorded almost all kinds of hazards; earthquake, droughts, extreme temperatures, floods, landslides, epidemics, wind storms, wild fires, insect infestations, mass movement wet, mass movement dry and volcanoes. Table 1.1 shows the distribution of affected people statics due to phenomenon occurred in Turkey between 1980 and 2010. Table 1.2 shows the distribution of killed people statics in Turkey owing to phenomenon occurred between 1980 and 2010.

Table 1.1. Distribution of affected people (taken from Prevention WEB in 2013).

Affected People		
Earthquake*	:	169.393,17
Epidemic	:	126,67
Extreme Temp.	:	1.207,14
Flood	:	59.183,90
Mass Mov. Dry	:	1.069,00
Mass Mov. Wet	:	1.498,56
Storm	:	234,14
Wildfire	:	230,00

Table 1.2. Distribution of killed people (taken from Prevention WEB in 2013).

Killed People		
Earthquake	:	587,03
Epidemic	:	11,67
Extreme Temp.	:	14,29
Flood	:	19,07
Mass Mov. Dry	:	261,00
Mass Mov. Wet	:	40,56
Storm	:	10,00
Wildfire	:	3,00

It is easily said that earthquakes are the most dangerous natural catastrophe which influenced adversely the human beings both mentally and economically for all centuries, especially in Turkey located one of the most seismically active regions. Earthquakes occur due to the deformation along the crust. In order to understand as much as possible all about earthquakes, studies of monitoring crustal deformation have been conducted by geoscientists with different backgrounds. Today, Interferometric Synthetic Aperture Radar (InSAR) is the most popular system to monitor crustal deformation.

InSAR is a new geodetic technique for determining earth topography and deformation and it does not need any land survey. Geophysical applications of radar interferometry take advantage of the phase component of reflected radar signals to measure apparent changes in the range distance of ground reflectors, that is, the land surface (Gabriel *et al*., 1989).

At the same time, unlike other methods, this technique provides a wide workspace and provides with a sensitivity of centimeters. This technique has an exclusive pixel density at the line of sight and ~ 1 cm accuracy (Massonnet and Feigl, 1998). SAR systems use microwave radar, by this circumstance, it supplies in every type of weather, on day-

night monitoring the geometrical and electrical specialties of the surface (Rosen *et al.*, 1998).

Since the launch of ERS-1 in 1991, InSAR has become a widely used technique for mapping the deformation of the Earth's surface caused by earthquakes (Massonnet and Feigl, 1998). In order to examine InSAR technique, Karlıova area is selected. In Karlıova, there were many earthquakes larger than magnitude four. In Table 1.3, the earthquakes which occurred in Karlıova, is listed.

Table 1.3. Important earthquakes that occurred in the study area (between 12.03.2005-26.08.2007).

Date	**Lat (N°)**	**Lon(N°)**	**Dept. (km.)**	**Magnitude**
12.03.2005	39.39	40.85	8	5.4
12.03.2005	39.39	40.90	16	4.2
14.03.2005	39.35	40.87	10	5.9
14.03.2005	39.40	40.82	14	4.9
15.03.2005	39.41	40.83	8	4.2
18.03.2005	39.37	40.87	6	4.2
18.03.2005	39.41	40.76	12	4.0
23.03.2005	39.37	40.81	10	5.4
23.03.2005	39.39	40.79	10	4.9
25.03.2015	39.43	40.72	4	3.9
02.04.2005	39.39	40.83	4	4.0
06.06.2005	39.37	40.93	8	5.7
10.08.2005	39.35	41.09	6	4.3
10.12.2005	39.38	40.86	18	5.2
02.07.2006	39.31	40.94	6	4.9
21.07.2006	39.37	40.82	4	4.1
26.08.2007	39.26	41.04	5	5.1

Karlıova (Bingöl) region is located between 38.00º-40.50º N Latitudes and 38.50º-43.50º E Longitudes. This region occupies an area on Alp Mountains belt extending from Azores Island to Indonesia region with it's of the geological structure and morphotectonic features. All the earthquakes, occurring in the area, are under the effects of the active faults. In Karlıova the annual mean maximum magnitude is 4.8 magnitudes and annual mean seismic risk is 74 percentages in the mentioned area (Sezer, 2008).In Figure 1.1, the earthquakes which occurred between 1949-2005 in Karlıova, is showed.

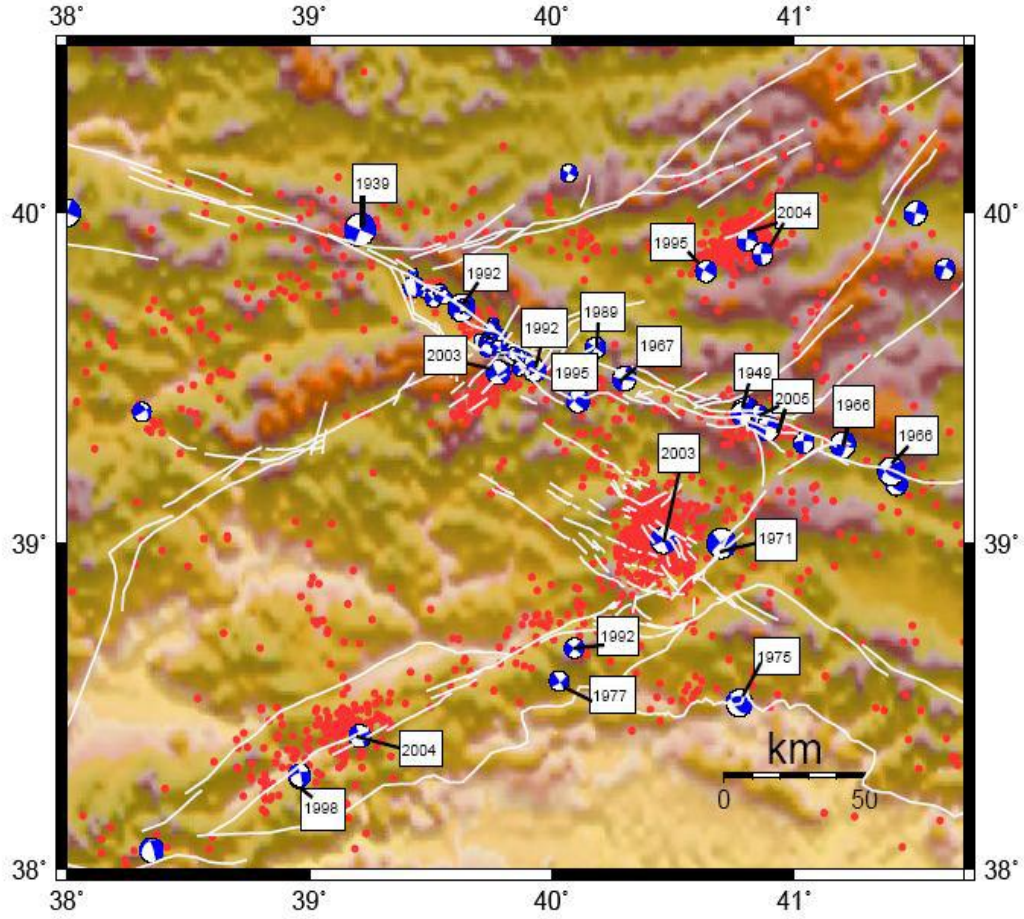

Figure 1.1. Significant earthquakes between 1949-2005 (taken from http://users.uoa.gr/~aagalos/Presentations_Posters/NH_Agalos_Ses6_1845.pdf).

The difference between the phases of two radar images is calculated in order to get the distance change during the time span of the two acquisitions. The calculated phase differences between the two images are called as interferogram, showing fringe defines the

changing of the coordinates on the ground. InSAR gives an opportunity to obtain three-dimensional information about the Earth's surface.

The second chapter gives some definitions used in this study about the SAR. Besides, the historical development of SAR, microwave radar, orbits and spacecraft, SAR techniques are explained in this section.

The third chapter gives some definitions about InSAR. Besides, factors influencing InSAR measurements, differential interferometry and InSAR techniques are explained in this section. The fourth chapter of this study explains methods of the study and data selection.

The last chapters assign the comments of analyses in a perspective of planning.

1.1. Study Area and Seismicity

Anatolian Plate, which is squeezed by the movement of Eurasia, Africa and Arabian Plates, has major active fault zones; North Anatolian Fault Zone (NAFZ) and East Anatolian Fault Zone (EAFZ).

NAFZ is situated at a point where two of the Earth’s tectonic plates meet, the Eurasian and Anatolian plates. The 1.200 km long NAFZ runs along the northern part of Turkey, from Karlıova in the east to the Gulf of Saros in the west and connects the East Anatolian compressional regime to the Aegean extensional regime. This study focuses on the Eastern Turkey(Figure 1.2). The active tectonics of Eastern Turkey is mainly dominated by the right-lateral NAFZ (Şengör, 1979; Dewey and Şengör, 1979; McClusky *et al*., 2000), running from Karlıova in the NE to İstanbul in the NW and left-lateral EAFZ (McKenzie, 1972; Jackson and McKenzie, 1988; Aksoy *et al*., 2007), running from Karlıova in the NE to Hatay in the SW.

The EAFZ was first described by Allen, (1969) and mapped by Arpat and Şaroğlu, (1972). According to Over *et al*. (2004) and Yilmaz *et al.* (2006), the EAFZ extends from

the Karlıova Triple Junction where it joins the NAFZ toward the southwest for about 600 km to the Kahramanmaraş triple junction near Antakya, where it joins the Dead Sea Fault Zone (DSFZ) (Şengör *et al.*, 1985; Westaway, 2004).

The EAFZ comprises several distinct strands with localized pull-apart basins and push-up zones rather than a through going continuous fault plane (Şengör *et al*., 1985; Westaway, 1994; Emre *et al*, 2005). Based on fault geometry and strike of the strands, the EAFZ consists of five (Hempton *et al*., 1981) or six segments (Şaroğlu *et al., 1992*). The age of the fault zone remains to be controversial, but it likely formed between Late Miocene-Early Pliocene (Şengör *et al.*, 1985; Hempton, 1987) to Late Pliocene (Emre *et al.*, 2005). Left-lateral displacement along the EAFZ is also confirmed by seismological observations (McKenzie, 1972) and geological studies (Şaroğlu *et al.*, 1992). In Figure 1.3, seismicity of the study area is shown.

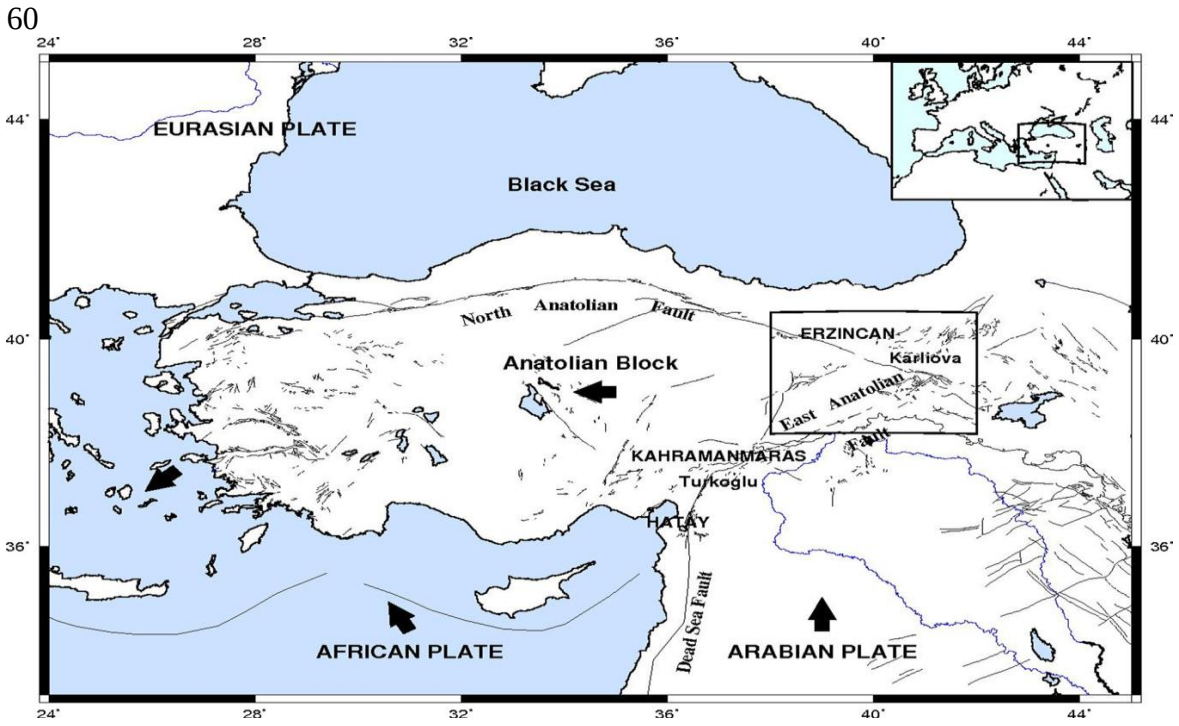

Figure 1.2. Tectonic setting of Turkey. Bold arrows show direction of plate motion (Özener *et al.*, 2010).

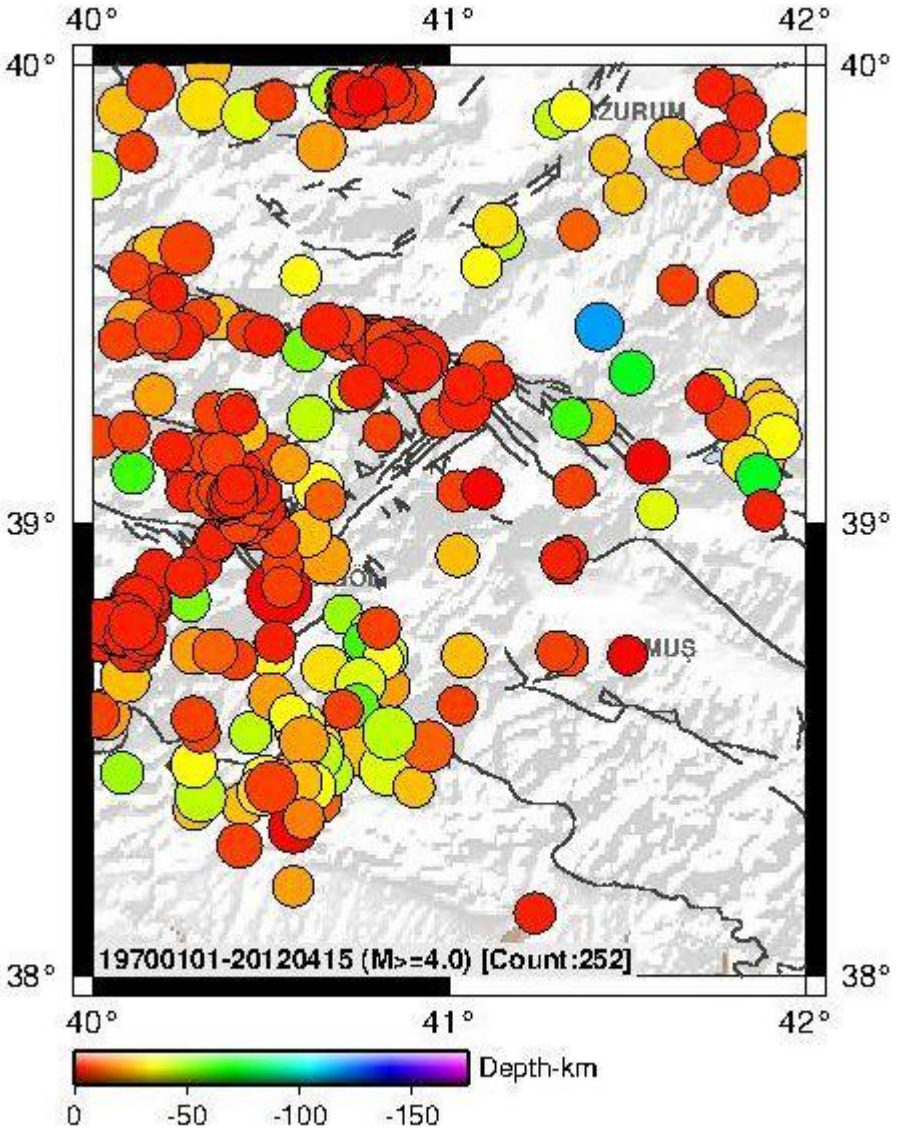

Figure 1.3. Seismicity of the study area between 1970-2012 (Source KOERI-NEMC).

The Northeast Anatolian Fault as a wide shear zone consists of many branches of faults which are parallel to each other, NE-SW oriented, left lateral and transformed.

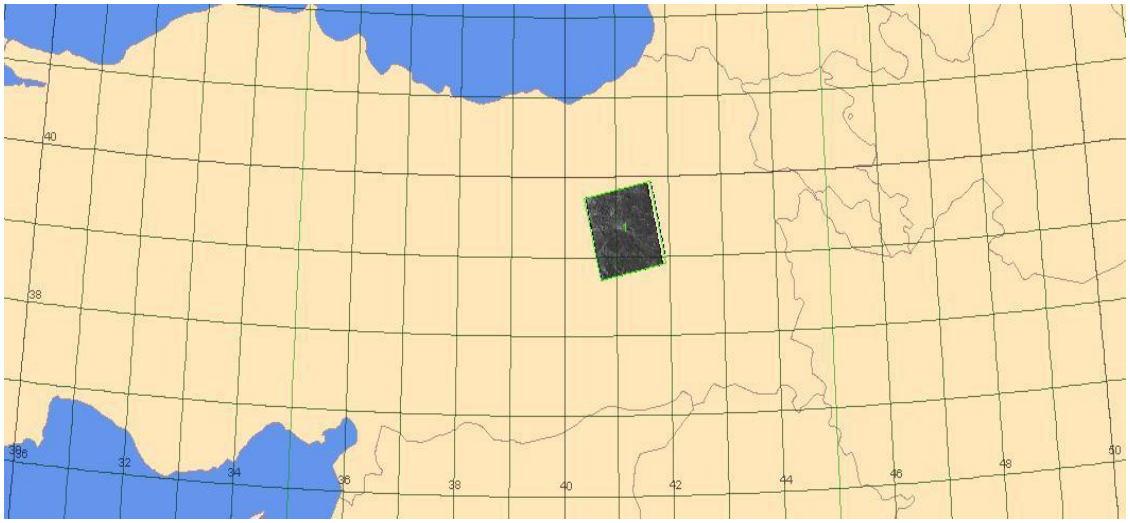

Figure 1.4. Study area and its vicinity (SAR images coverage on the ground).

Earthquakes occurred in Karlıova region which shown in Figure 1.4 created by Eolise program. Those earthquakes were felt in a wide area involving central distinct Karlıova, Bingöl, Muş, Erzincan and Erzurum. Some buildings were destroyed and some were damaged moderately and lightly in Karlıova. (Gülkan *et al*, 1993).

2. SYNTHETIC APERTURE RADAR (SAR)

RAR transmits pulses from a side-looking antenna and are airborne rather than satellite borne. The azimuth spatial resolution is dependent on the antenna footprint and is linearly proportional to the distance between the sensor and the surface. For high spatial resolution requirements in spaceborne platforms, this technique is not viable because the antenna would need to be impractically large (Elachi, 1987). SAR is developed in order to eliminate the limitations of RAR systems.

The synthetic aperture imaging technique in a SAR uses the movement of the sensor to simulate a much larger antenna than its actual size. A single antenna moving along the flight line acquires the data and the effect is similar to using an array of antennas. The target is illuminated several times from different locations generating numerous echoes that are recorded coherently (*i.e.*, amplitude and phase as a function of time) and subsequently combined to synthesize a linear array. A higher spatial resolution is achieved independently of the distance between sensor and target and by a small antenna (Elachi, 1988). SAR systems can be either airborne or spaceborne and are much more complex than the RAR systems.

SAR generates fine azimuth resolution by utilizing long wavelengths and short antenna heights. In addition, the azimuth resolutions of those systems are independent of angular distance. SAR imagery has the big advantage of being able to collect data in order to investigate terrain changes regardless of the geography of the region (Akabalı, 2002).

As shown in Figure 2.1, the (P) terrain point is displayed by starting from the point A position to the point B position. Thus, (P) terrain point is detected from various locations during the motion of the radar from point A to B.

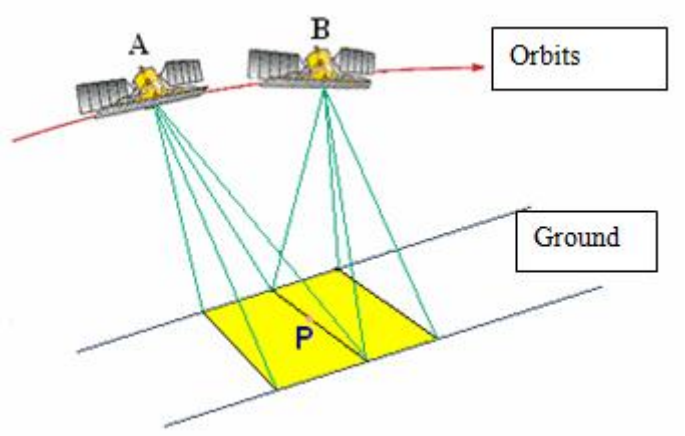

Figure 2.1. SAR system (Köse, 2006).

2.1. Historical Background

Radar was developed by the United States of America during 1920s as a tool for ship and aircraft detection. However, those radars were only ground-base radars. Systems for tracking and detection of aircraft were developed during 1930s. Due to requirement of impractical long antenna lengths of those types of radars, SAR was being developed during 1950s.

First type of SAR radars were processing the backscattered echoes from the target by utilizing optical (analog) processors and image processing was accomplished by using Fresnel approximations (Cutrona, 1966). First applications of SAR interferometry were used to study the surface of Venus and the Moon (Rogers and Ingalls, 1969; Zisk, 1972 a.b).

SAR dates back to 1960s where the interferometry principle, used in radio astronomy, is first applied over places like the Darien province of Panama (MacDonald, 1969).

During 1970s, an alternative SAR imagery method called Polar Format Processing which is based on Plane-Wave Approximation technique was suggested for InSAR providing high resolution mapping (Ausherman, 1984). Graham was the first to introduce

the technique for topographic mapping in 1974 by using an airborne SAR system configured as a cross-track or vertical interferometer (Çakır, 2003).

In attempt to oceanographic researches, the satellite Seasat was sent into space on June 26, 1978 by NASA enabled Earth imaging by SAR method (Massonet ve Feigl, 1998).

The use of space borne SARs as interferometers (InSAR, DInSAR or IFSAR) became popular only recently, although the basic principle dates back to the early 1970s (Graham, 1974).

However, in view of terrestrial applications it was only in the 1980s that the first results were published by Gabriel *et al.,* (1989), Goldstein *et al.,* (1989), Goldstein and Zebker, (1987), Goldstein *et al.,* (1988), Zebker and Goldstein, (1986).

Goldstein and Zebker (1987) first employed an along-track InSAR configured to measure radial velocity. They used two horizontally separated antennas to receive backscattered signals from the moving sea surface. Gabriel and Goldstein (1988) first demonstrated single-antenna, repeat-pass interferometry by using data collected on two separate passes of the Shuttle Imaging Radar.

The first study demonstrating the InSAR method is a useful tool to measure movements of Earth was published by Gabriel *et al,.* (1989). As mentioned earlier, during the researches about Landers Earthquake in California, the number of geologists using SAR method began to increase rapidly. In the 1990s, the SAR systems had began to be sent into space by setting them up into Satellite Platforms. Thus, monitoring and displaying on larger areas were made possible successfully.

However, after the launch of the ESA satellite ERS-1 in 1991 an enormous amount of SAR data sets suitable for interferometry, became available and a series of research groups began to investigate the method intensively and with success.

Today it is generally appreciated that SAR interferometry is an extremely powerful tool for mapping the Earth's land, ice and even the sea surface topography. The so-called differential InSAR method (D-InSAR) represents a unique method for detection and mapping of surface displacements over large temporal and spatial scales with precision in the cm and even mm range.

2.2. Radio Detection and Ranging (Radar)

Radar is an object detection system. The systems or devices which operate by transmitting electromagnetic waves onto target objects and amplifying the signals the target object reflects, hereby making the detection of the target possible are called as radars (Akoğlu, 2001).

Those systems provide the big advantage of detection and also calculation of ranges of targets. Radars had begun to take place in history by the suggestion of Electro-Magnetic Wave Theory and Electro-Dynamic Theory of Light by James Clerk Maxwell in 1865 and by the discovery of electro-magnetic waves by Hertz in 1866 (Akoğlu, 2001).

Unlike optical and infrared imaging sensors, which relay on reflected or radiated energy (*i.e.* the Sun), radar is an active sensor, which provides its own illumination in the form of microwaves. Microwaves are electromagnetic waves in the 1-1.000 GHz region of the electromagnetic spectrum which is shown in Figure 2.2.

Since electro-magnetic waves are the fundamental basis of operation of radar system, it is a necessity to mention electro-magnetic waves briefly. The electro-magnetic wave is a form of wave which propagates in the space and keeps wave like behavior in vacuum. It has both electric and magnetic field components which oscillate in a phase perpendicular to each other and perpendicular to direction of wave propagation in a sinusoidal pattern (Akoğlu, 2001).

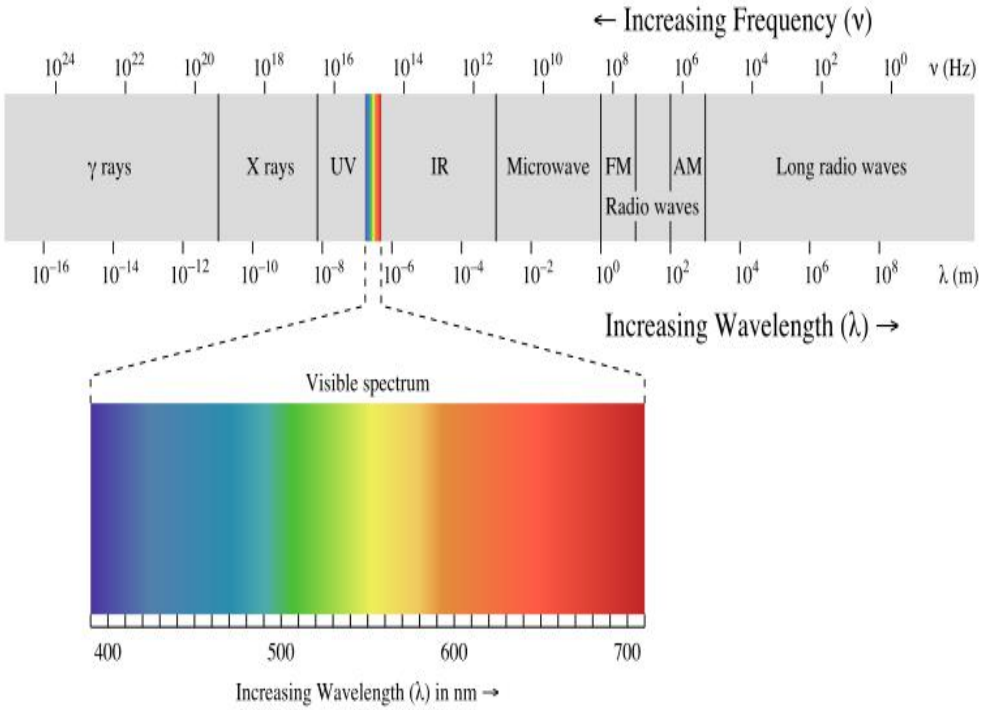

Figure 2.2. Microwave frequency bands (Radar Tutorial).

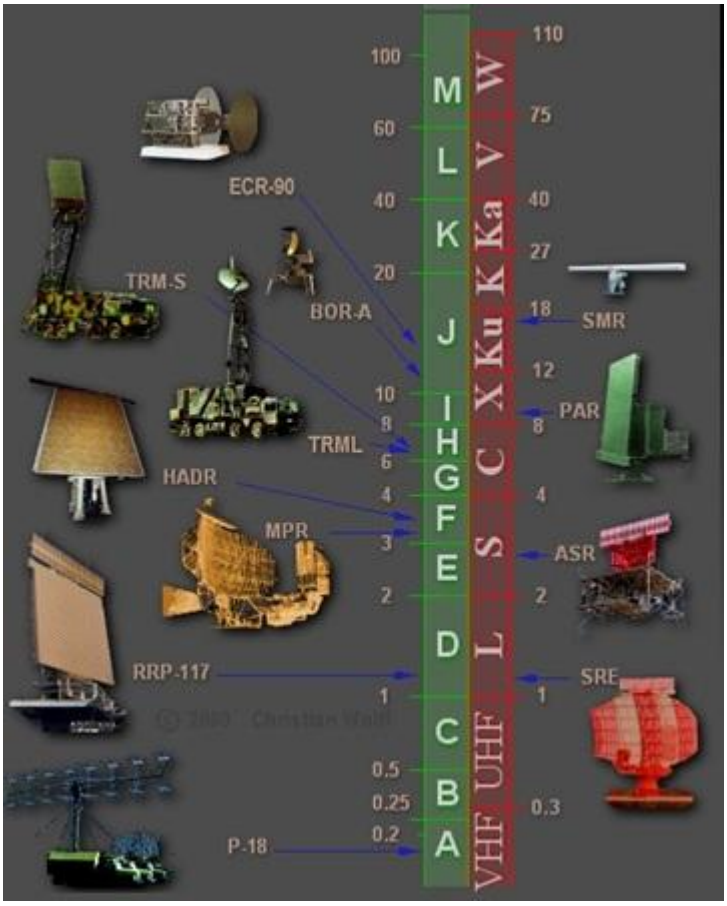

Figure 2.3. Radar and frequency bands (Radar Tutorial).

SAR systems transmit the microwaves towards the area to be imaged. Those systems transmit the microwaves towards the area to be imaged, collect returned echoes and calculate the travel time depending on the strength of returned signals. This process allows detecting order of objects (Dilia and Domingo, 1999). Figure 2.3 shows the microwave frequency bands.

The SAR radar antenna is used for both sending and receiving microwave signals. This antenna operates by sending microwave signals between frequencies 300 MHz to 30 GHz correspond to 1 cm to 1 m wavelengths to the area to be imaged and also by receiving returned signals from the target in the same frequency interval (Curlander, 1991).

The Advantages of Radar Imaging System which used for the InSAR technique are listed as follows:

- Radar Imaging System is an active system. In other words, it has the ability to produce the energy it requires by itself. For this reason, Radar Imaging System provides the advantage of imaging through any type of weather condition and can be used in the day or night time.
- It detects the changes in surface topography and morphological changes in marine and ground environments sensitively.
- It provides high sensivity detection for water and relative humidity.
- It provides the advantage for underground researches depending on the density of the ground and moisture.

Radar Imaging System displays an image which is defined by pixel value numerically depending on the strength of returned echoes from the ground (Akabalı, 2002).

There are some parameters that affect the reflection of radar systems. Those are listed as follows:

- Observational parameters of the radar technology (such as frequency, polarization, angle of incidence of reflected signals.
- Physical parameters of Earth (such as ratio of surface roughness, geometric shape, moisture content).

2.3. Satellites and Orbits

Radar Systems transmit and receive the electromagnetic waves in the range X (3 cm), C (6 cm) or L band (24 cm). Electromagnetic waves at bandwidth mentioned propagate along the atmospheric layers without significant energy losses regardless of air conditions. Today's, for the interferometric applications, there are some important satellites.

Table 2.1. Satellites.

Satellite	Date	Band	Institution
SeaSAT	1978	L	NASA
SIR-B*	1984	L	NASA
ERS-1	1991-2000	C	ESA
JERS-1	1992-1998	L	NASDA
SIR-C/X-SAR	1994	K/C/X	NASA/ASI
ERS-2	1995-....	C	ESA
RADARSAT-1	1995-...	C	CSA
SRTM	2000	C/X	JPL/NASA/NIMA/DLR/ASI
ENVISAT	2003-2012	C	ESA
ALOS	2006-....	L	JAXA
RADARSAT-2	2007-....	C	CSA
COSMO SkyMed	2007-....	X	ASI
TerraSAR-X	2007-....	X	DLR/EADS

SAR has been shown to be very useful over a wide range of applications, including sea and ice monitoring, mining, oil, pollution, monitoring, oceanography, classification of earth terrain, geological deformations, plate boundary deformation as shown in the reports of European Space Agency (ESA), JERS of Japan, Radarsat Satellites of Canada and SIR-C/X-SAR shuttle flights. Satellites which are used frequently are mentioned in Table 2.1.

2.3.1. Envisat (European Environment Satellite)

Envisat is by all accounts a huge satellite. It is about 30 feet long (9 meters) and 16 feet wide (5 m). The spacecraft weighs 17,600 pounds (8,000 kilograms) and has a huge sail-like solar array that is 16 feet wide (5 m) and 46 feet long (14 m).

In 2010, space debris experts said that the satellite's immense size will make Envisat a major space junk risk for up to 150 years.

ESA launched the Envisat mission in 2001 to study the Earth from space in extreme detail. The satellite carries 10 sensors to study Earth's oceans, land, ice caps and atmosphere and has been a vital resource for about 2,500 scientific studies of our home planet.

More advanced imaging radar, radar altimeter and temperature-measuring radiometer instruments extend ERS data sets. This is supplemented by new instruments including a medium-resolution spectrometer sensitive to both land features and ocean color. Envisat also carries two atmospheric sensors monitoring trace gases. It carries ten sophisticated optical and radar instruments to provide continuous observation and monitoring of the Earth's land, atmosphere, oceans and ice caps. Envisat data collectively provide a wealth of information on the workings of the Earth system, including insights into factors contributing to climate change (ESA, 2013).

Its largest single instrument is the Advanced Synthetic Aperture Radar (ASAR), operating at C-band, ensures continuity of data after ERS-2. It features enhanced capability in terms of coverage, range of incidence angles, polarization, and modes of operation. The improvements allow radar beam elevation steerage and the selection of different swaths, 100 or 400 km wide (ESA, 2013).

The ASAR instrument is operating at C-band and provides both continuity to the ERS-1 and ERS-2 mission SARs and next generation capabilities in terms of coverage, range of incidence angles, polarization, and modes of operation. The resulting

improvements in image and wave mode beam elevation steerage allow the selection of different swaths, providing swath coverage more than 400 km wide using ScanSAR techniques. ScanSAR is a SAR technique that combines large-area coverage and short revisit periods with a degraded spatial resolution compared to conventional SAR imaging modes.

ASAR can provide a range of incidence angles ranging from 15° to 45° and can operate in alternating polarisation mode, providing two polarization combinations (VV and HH, HH and HV, or VV and VH). The ASAR is onboard the Envisat satellite, which was launched into a sun-synchronous orbit in March 2002. The exact repeat cycle for a specific scene and sensor configuration is 35 days. In Table 2.2, the properties of the ASAR satellite are shown. Figure 2.4 shows the Envisat satellite.

Table 2.2. ASAR properties.

Mode	**Id**	**Polarisation**	**Incidence**	**Resolution**	**Swath**
Alternating polarisation	AP	HH/VV, HH/HV, VV/VH	15 – 45°	30 – 150 m	58 – 110 km
Image	IM	HH, VV	15 – 45°	30 – 150 m	58 – 110 km
Wave	WV	HH, VV		400 m	5 × 5 km
Suivi global (ScanSAR)	GM	HH, VV		1 km	405 km
Wide Swath (ScanSAR)	WS	HH, VV		150 m	405 km

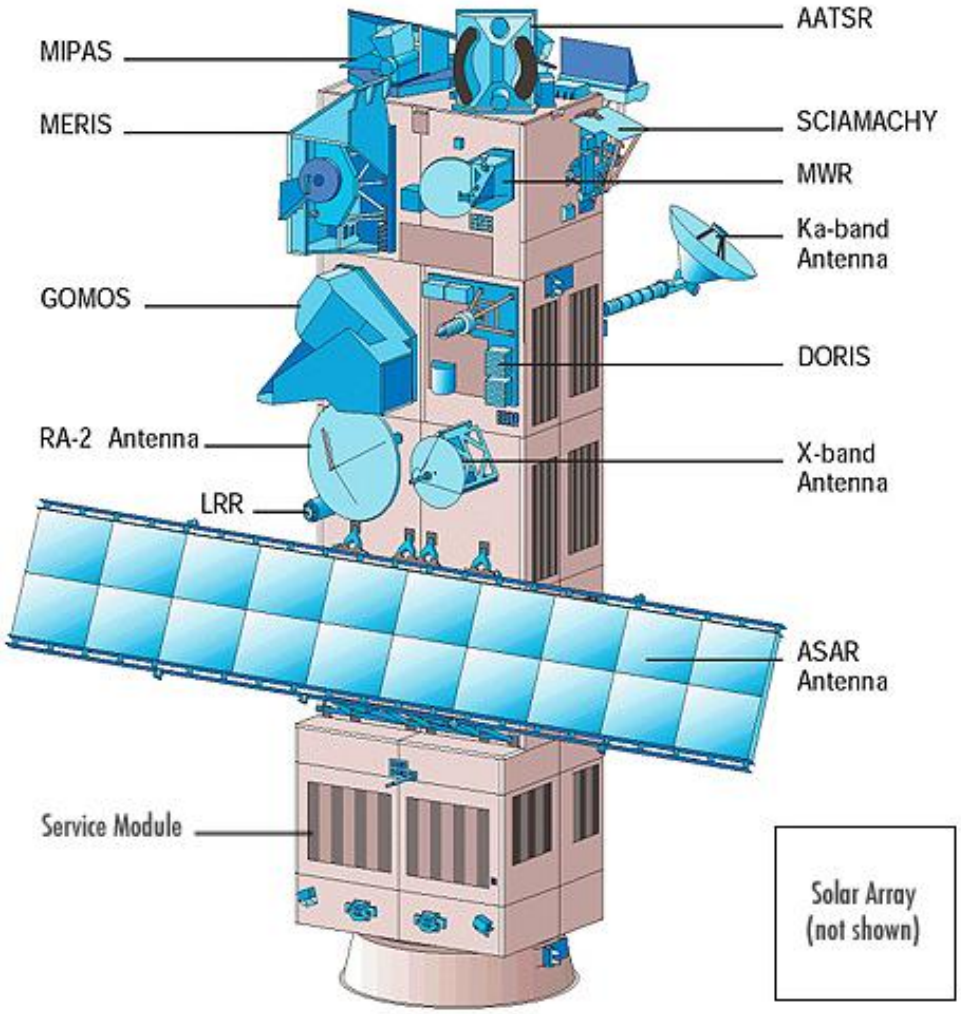

Figure 2.4. Envisat (ESA, 2013).

2.4. Geometry of Synthetic Aperture Radar

SAR is a radar system which utilizes the flight path of the platform to simulate an extremely large antenna and aperture electronically. Over time, individual transmit-receive cycles (PRT=Pulse Repetition Time) are completed with the data from each cycle stored electronically. The signal processing uses magnitude and phase of the received signals over successive pulses from elements of a synthetic aperture. After a significant number of cycles, the stored data is recombined to create a high resolution image of the target. This process is completed by taking into account Doppler Effects in case of defining target geometry. Thus, a high angular resolution radar picture is obtained which real aperture radar cannot creates.

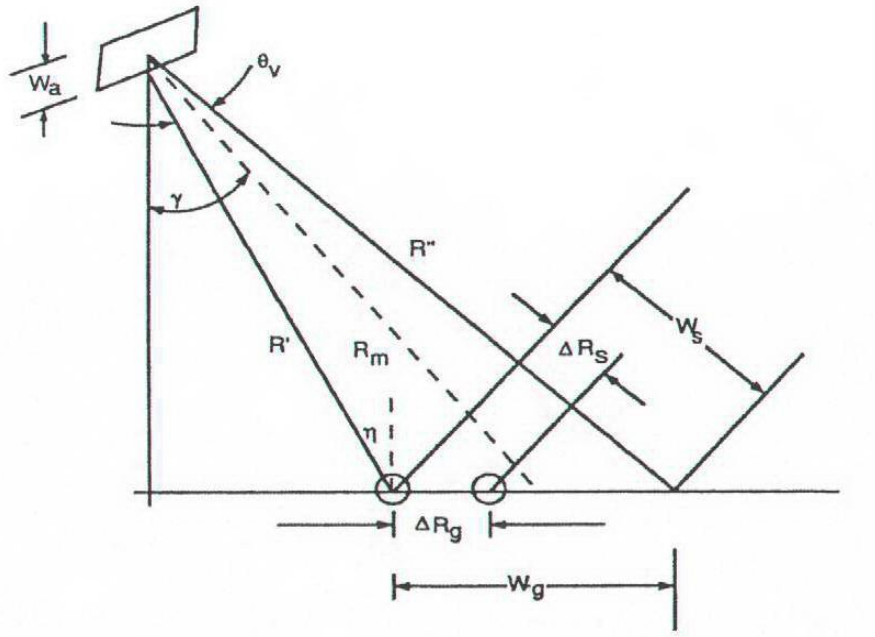

Figure 2.5. SAR geometry (Curlendar and McDonough, 1991).

In Figure 2.5, viewpoint angle "γ" due to vertical line and the angle between the radar beam and the surface normal is equal to reflection angle "η". This is because of the earth surface which is assumed to be straight. Radar transmits electromagnetic energy as electromagnetic pulses. Reflected waves are stored and sampled in order to process signals afterwards. The azimuth direction of radar corresponds to flight direction and the range direction corresponds to perpendicular direction of the azimuth direction. "W_g" size of the radar beam (Swath width) which identifies the vertical wave width W_A is determined by antenna height. If "R_m" is the distance to the center of the swath,

$$W_{g=(}\lambda R_{m)}/(W_a \cos \eta) \tag{2.1}$$

Range resolution is,

$$\delta R_{g=(}\lambda R_{m)}/(2B_r \sin \eta) \tag{2.2}$$

Br is the impact band width.

The most significant property of SAR which gives it an advantage than other systems is the resolution towards azimuth direction (Akoğlu, 2001).

In practice, Doppler Shifts are detected by transmitting coherent, periodic pulses and by calculating time history (FFT) of each range bin. This method is one of the easiest and prevalent methods (Webb *et al.*, 1998).

Doppler Frequency is defined as the difference in frequency of a wave for an observer moving relative to its source. For example, two objects moving in the same path as the radar are expected to have different relative velocities at any time due to moving platform. Indicated relative velocity would be determined due to radar moving relative to its source. For this reason, radar waves reflected from two objects would have different Doppler Frequencies. Doppler Frequency is related to coordinates of details. This could be reached by analyzing recorded signals in the radar.

Consequently, the details even having the same R distance regardless of their presence in the same ray beam could be determined separately by analyzing Doppler Frequency Spectrum. By the help of Doppler Frequency (f_{Do}) and pulse repetition time (PRT), 2D mapping of targets and determination of their coordinates could be enabled. $\tau_0=2R_{(0)}/c$ corresponds to a circle and Doppler Frequency (f_{Do}) corresponds to a hyperbole. Those two figures intersect at four points of range plane with a distance "x". Left/Right uncertainty could be clarified by the help of the direction of the radar beam oriented. An Arm of Hyperbola is determined by the signal of Doppler Shift. In this case, azimuth resolution is given as;

$$\delta x_{=(}\lambda R/2V_{ST)}/(W_a\ V_{ST}/R\lambda)=L_a/2 \qquad (2.3)$$

is indicated as relative velocity, "Wa" is the length of radar antenna towards flight direction, "R" is angular distance between the radar and target and "λ" is indicated as wavelength (Şengün, 2009). In radar imaging, it is possible to encounter some effects due to both topography of the region and radar parameters such as foreshortening, layover and shading.

2.4.1. Foreshortening

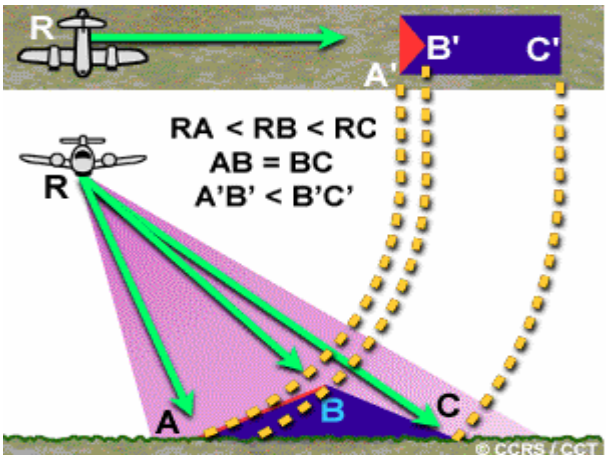

Figure 2.6. Foreshortening (CCRS).

Figure 2.6 shows that the peak of a mountain b has the same slope with respect to A and C bottom points. Horizontal distance between the points A and B of the mountain appears to be shorter than B-C horizontal distance which substantially have the same distance as A-B.

The reason for this, a bottom point is the closest point to the radar thus it enters first. B peak point appears to be closer to the point A in the image on the other hand C point is expected to have a larger reflection time and as a result of this, A point looks more distant. The relative difference in radar image is called as “foreshortening”. Scale Corruption (Foreshortening) could be eliminated by using oblique distance and platform heights by the help of geometry (Şengün, 2009).

2.4.2. Layover

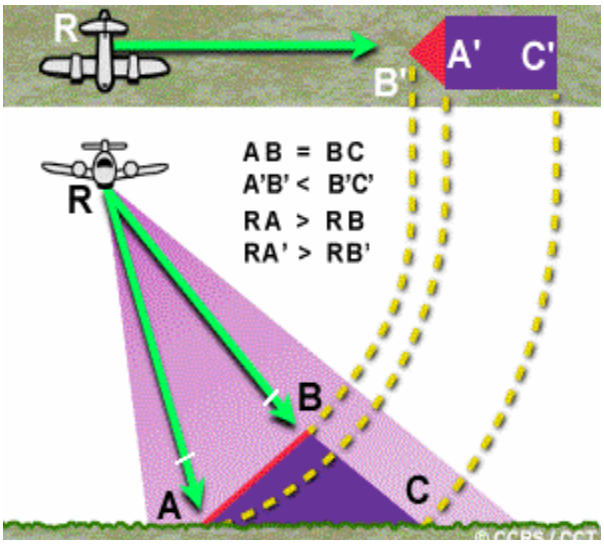

Figure 2.7. Layover (CCRS).

Layover occurs when oblique distance B peak of the mountain have a compressed slope compared to A bottom point (Figure 2.7). Due to the signal reflected from the top that returns faster than the signal reflected from the bottom, A-B range is to be reversed. This range is represented as A'-B' incorrectly.

If the radar shadows of two same sized objects are compared, the distant one is expected to appear longer than the closed one. Shaded regions appear darker (Zero signal). Any data collection from such an area is only caused by system noise (Şengün, 2009).

2.4.3. Shadowing

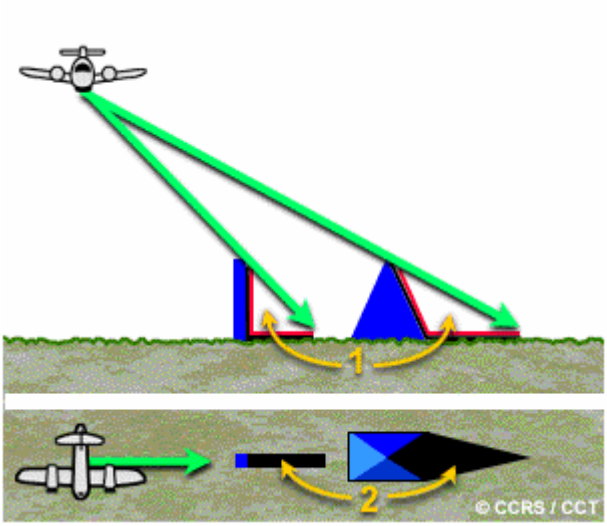

Figure 2.8. Shadowing (CCRS).

The shadowing effect that shown in Figure 2.8 occurs when the incident angle of radar antenna is smaller than the slope of the terrain. Shaded region appears darker in radar images. Because of this reason, it is not possible to catch details behind the shadows (Köse, 2006).

3. INTERFEROMETRIC SYNTHETIC APERTURE RADAR

3.1. Technique of InSAR

Geodesy is the key factor in order to determination of deformation and velocity vectors. Area based or point based significant movements, their velocities directions could be determined with the help of terrestrial or spatial measurements. For this purpose, spatial techniques such as VLBI (Very Long Baseline Interferometry), SLR (Satellite Laser Ranging), LLR (Lunar Laser Ranging), InSAR and GPS (Global Positioning System) and terrestrial techniques such as classical angle measurements are used.

The term interferometry is derived from the word "interference". Interference is a phenomenon that occurs when has waves of any kind such as, sound, light, ocean, electromagnetic, seismic waves and *etc*. Interference occurs whenever two waves together. InSAR method is a method in which the phenomenon of interference is combined with SAR (Çakır, 2003). SAR is an active sensor, transmitting its own energy, and then measuring the return scattered by the Earth's surface back to the satellite's antenna (Aklıouat *et al.*, 1980).

GPS is a useful technique for the determination of pre-seismic (before earthquake), co-seismic (earthquake moment) and post-seismic (after earthquake) terrestrial movements. GPS is applied commonly on determination of accumulation of stress before earthquake, measurement of moment magnitude at earthquake moment and the effect of the elastic movement on the region after the earthquake (McClusky *et al*., 2000).

On the other hand, lnSAR enables identification of velocity field of a region and estimations before and after the earthquake. There is a basic difference between these two methods caused by their velocity components. GPS method has higher accuracy on determination of horizontal velocity component and InSAR has higher accuracy on determination of vertical velocity component (Hanssen, 2001). Although it is difficult to collect data by GPS method, it provides better data processing. Besides, it is easier to

collect data by lnSAR method but more difficult data processing (Yavaşoğlu and Tarı, 2011).

InSAR method is also applied in order to measure deformations on terrestrial surfaces. Interferograms belonging to the Landers Earthquake that occurred in California in 1992 that obtained by the help of ESR Images which were displayed by European Space Agency (ESR) are the first examples showing that lnSAR method has a great potential as a geodesic tool. The technique was being developed for diverse range of applications at the same time.

High resolution could be achieved by utilizing a small antenna which could form SAR successfully (Uslu, 2002). As airborne or space borne side looking SAR system moves in its flight path in order to image a swath, it records phases and amplitudes of the returned echoes from the Earth surface (Zebker *et al*., 1994).

Thanks to space borne side looking radars displaying detailed images of the surface hereby provides a more detailed research. This shows superiority of satellite images which provide practical solutions on geology. A consideration upon new generation satellites such as Envisat, Radarsat, ALOS, width of the swath could be increased to 400 km/s by moving side looking antenna up and down by respect to orientation of target (Widecan SAR and ScanSAR).

Thus, even though the standard size of SAR Images is 100 x 100 km, it is possible to ensure 400 x 400 km sized images by using advanced radar systems. Satellites have the capability of viewing a region both descending from north to south and ascending south to north once a month (Çetin, 2010).

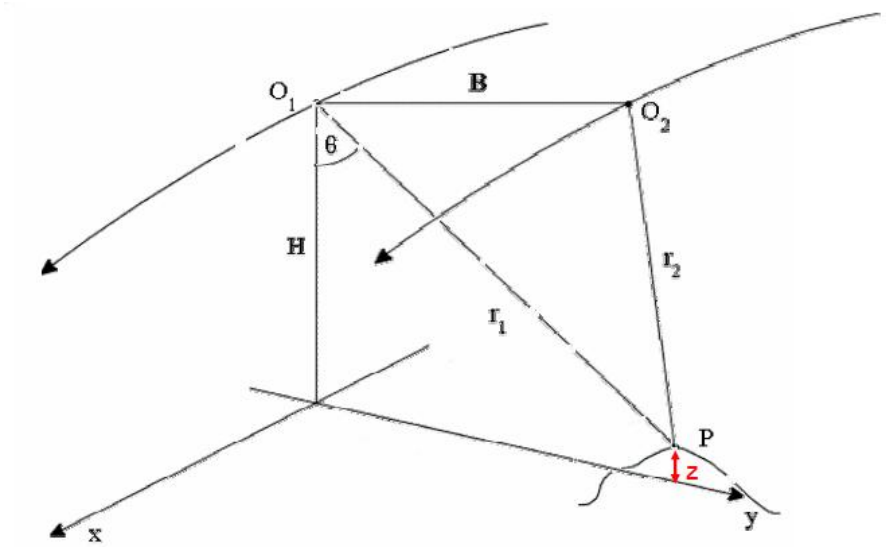

Figure 3.1. Position of satellite and ground (ASF).

In the case of viewing the same object by utilizing O_1 and O_2 antennas (Figure 3.1), it is possible to measure side looking distances (Range for O_1 antenna is r_1 and for O_2 antenna is r_2.). If viewpoint "φ" and height of flight "H" are known, it is easy to reach to "z" (X, Y) parameters by the help of triangle-edge calculations.

The difference between the phase values of two different radar images of the same region, assuming that the characteristic of Earth reflection remains the same and neglecting random factors, correspond to distance difference of two different moving radars. Delay in atmospheric distance cause the phase difference indicated (Wright, 2000).

Interference refers to the interaction of waves that are correlated or coherent with each other. The pattern that is created by two interacting waves with a phase difference is called "interferogram". Interferogram is considered as an interference pattern calling brighter or darker lines depending on the wave orientation. Brighter lines refer to constructive interference and darker lines refer to destructive interference. In a study carried out in order to determine the deformation; The effect of topography independent of atmospheric factors could be eliminated by the help of DEM and the effect of imaging geometry could be eliminated by the help of satellite orbital data consequently it would be only the deformation that caused by phase difference remained (Şengün and Deniz, 2009).

The interferogram is an interference pattern of fringes due to relative phase difference. It is effectively a contour map of the change in the distance from the radar to the ground surface. Each cycle of phase, or fringe, in the resulting interferogram corresponds to a change in range distance from the satellite or aircraft to the ground surface equal to one-half of the radar wavelength (5.66/2+2.83 cm for ERS) (Çakır, 2003).

The distance between two flight paths is called baseline. For every SAR imaging system, there is a critical baseline length, above which interferometry becomes impossible (Zebker and Villasenor, 1992).

The distances between the antennas (baseline) belonging to radar orbits determine how to take advantage of those set of images. For example, in order to compose a digital elevation model from radar images, the distance between the images should be about 150-300 meters. In order to research surface deformations, the distance between antennas should be about 30-70 meters. Practically, this distance value should be less than 600 meters for interferometry (Solaas, 1944).

The distance between the antennas has a great importance especially for the sensitivity of topographic maps. It is one of the potential error sources and should be measured sensitively (Zebker *et al.*, 1994).

Basically, lnSAR technique takes the advantage of phase differences between SAR images in order to determine surface deformations and altitude as well. SAR processing is the transformation of raw SAR signal data into a spatial image. Fractional Surface deformations about centimeter levels which occur very slowly (days and years) could be easily determined by the help of this technique.

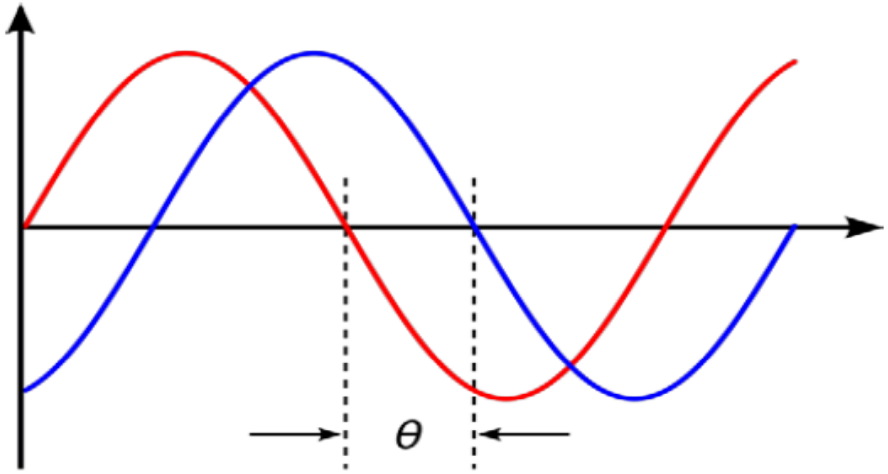

Figure 3.2. Phase difference.

After all, the radar transmits pulses at the pulse repetition frequency (PRF) and for each pulse the backscatter return from the ground is sampled in range at the analog to digital (A/D) sampling frequency. The radar operation is coherent, which means that both the return magnitude and phase (with respect to the transmitted signal shown in Figure 3.2) are sampled. For each range sample the in-phase and quadrature values (I and Q) are stored. The raw data file is thus a two dimensional array of complex values (with "I" as the real part and "Q" as the imaginary part). This two-dimensional data set is then processed to form an image (Aklıouat *et al.*, 2008).

In order to obtain SAR data, three main techniques are used. The main parameter that separate from each other is direction of the datum line. The other important thing is antenna location in the platform. They are across-track, along track and repeat-pass techniques.

3.1.1. Across Track

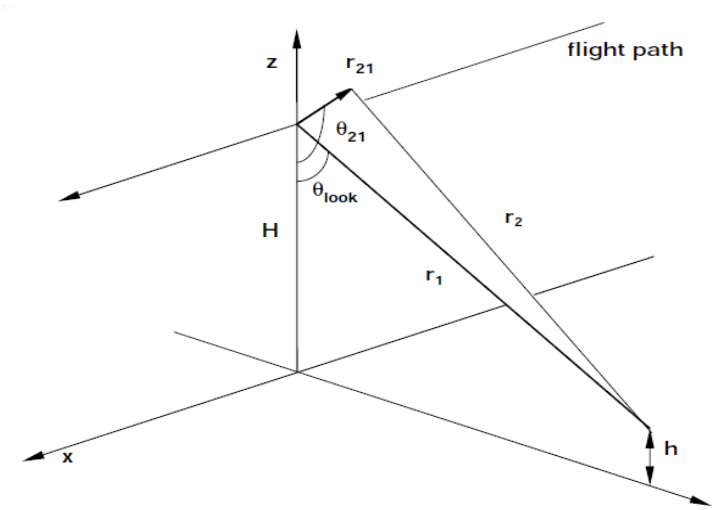

Figure 3.3. Across track (Gens, 1998).

Process is performed through two SAR antennas which are mounted on the same platform that shown in Figure 3.3. Height model could be obtained by unwrapping the phases. Topographic height "y" is calculated by $y=r_1 \sin\Theta$ formula (Akoğlu, 2001). This technique is often used in the researches that obtained by usage of aircrafts. For this reason, even master and slave images are obtained from different locations could be stored on the same date (Zou *et al.*, 2009).

3.1.2. Along Track

This technique is only practiced in aircraft type SAR applications because of the necessity of two SAR antennas. The technique had developed on the purpose of determination of ocean current directions and tracking moving objects.

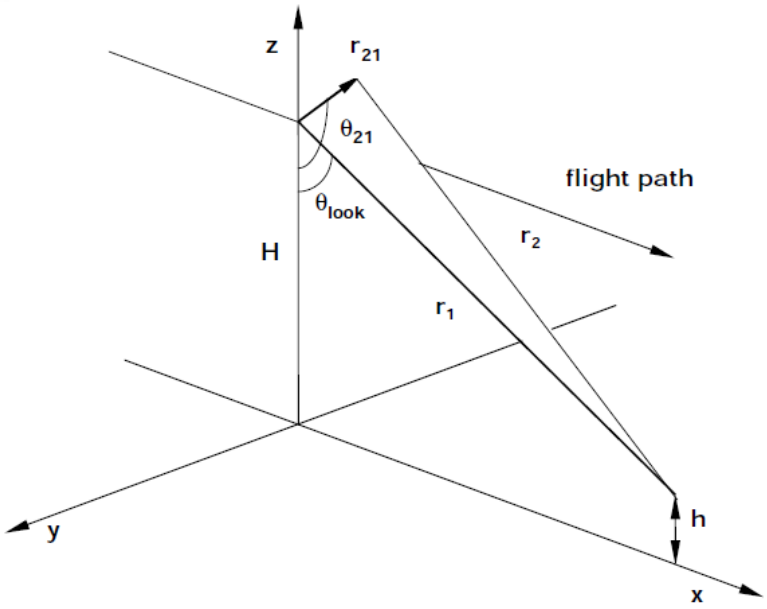

Figure 3.4. Along track (Gens, 1998).

Mathematical background of this technique is not different from the previous one. Only axis directions are different. A consideration upon sea currents, "φ" phase difference between the signals would be occurred by current flow that is shown in Figure 3.4. Moving Surface would cause a Doppler Shift due to phase velocity of sea waves. The technique provides only images of moving segments. The relationship between the velocity of an object or point and phase difference:

$$\varphi_{=(}4\pi/\lambda_{)}/(\mu/V)\ B_x \qquad (3.1)$$

Here, "v" represents the velocity of the aircraft, "λ" is wavelength and "B_x" represents base length. The sensitivity of interferometric measurements depends on the choice of the proper base. Neither of those two methods indicated above provide a proper base choice. This is expected result of two SAR antennas mounted on the same platform.

SAR processing significantly improves the resolution of point targets in both the cross-track (range) and along-track (azimuth) direction by focusing the raw radar echoes (Elachi, 1988; Curlander and McDonough, 1991).

3.1.3. Repeat Pass

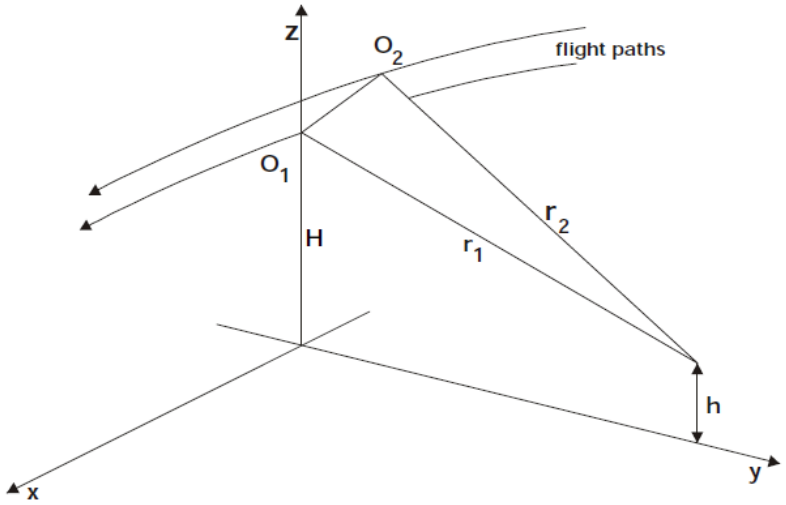

Figure 3.5. Repeat pass (Gens, 1998).

Repeat Pass technique (Figure 3.5) as it's evident from its name stores data through re-passing satellite. It has a great importance to determine flight trajectory exactly.

The distance between antennas could be measured by taking into account "B" base magnitude which is calculated from orbital locations of satellites or oblique target distances that are measured. The phase difference is calculated by formula shown above.

$$\Delta\varphi_{=(-}4\pi/\lambda)B \qquad (3.2)$$

3.2. Differential Interferometry

Radar differential interferometry is an up-to-date measurement technology. It is now possible to detect subtle changes in the Earth's surfaces over periods of days to years with a scale (global), accuracy and reliability (day or night, all weather) that are unprecedented. The basic principle of the technique involves interferometric phase comparison of a series of SAR images. To date many examples illustrate how SAR differential interferometry can be applied to the study of coseismic deformation generated by an earthquake (Gabriel *et al.*, 1989; Gens and Genderen, 1996).

Because of its unique capability, which no other technique provides high-spatial-resolution maps of earthquake deformation, these pioneering studies have generated enormous interest in the Earth science community because they point to an entirely new way to study the surface of the Earth.

Differential InSAR (DInSAR) technique enables the measurement of surface deformation with an accuracy of a few millimeters to centimeters for wide spatial coverage. Interferograms are generated by differentiating the phase values of two co-registered SAR images acquired at different times over the same area (Karimzadeh and Ahmedi, 2013).

In the field of tracking fault movements and land subsidence, various researches have been done using DInSAR. Some of them include investigations on North Anatolian Fault, Turkey (Wright *et al*., 2001; Çakır *et al*., 2005; Motagh *et al*., 2007; Walters *et al*., 2011), San Andreas Fault, U.S (Lyons and Sandwell, 2002), Altyn Tagh Fault, Tibet (Elliott *et al*., 2008), the subsidence of Mexico City (Osmanoğlu *et al*., 2011), the subsidence of Mashhad Plain, Iran (Motagh *et al*., 2006; Dehghani *et al*., 2009) and *etc*.

DInSAR has significant amount of useful data, such as surface deformations due to seismic events (Massonnet *et al*., 1993; Jacobs *et al*., 2002). It has applications for geophysical monitoring of natural hazards, for example earthquakes, volcanoes, landslides,

land subsidence and also faults (Liu *et al*., 2004; Pathier *et al*., 2003; Rosen *et al*., 2000; Motagh *et al*., 2006; Lanari *et al*., 2007; Çakır *et al*., 2007).

The DInSAR techniques exploit the information contained in the radar phase of at least two complex SAR images acquired in different epochs over the same area, and that form an interferometric pair.

SAR image contains two components per pixel, from which the amplitude and phase signal can be derived. The phase is the key observable of all InSAR techniques. The repeated acquisition of images over a given area is usually performed by using the same sensor, *e.g.* the Envisat ASAR, or sensors with identical system characteristics, as it is the case of ERS-1 and ERS-2. Only in particular cases it is possible to make cross interferometry by using images acquired with different systems.

In order to obtain coherent SAR image pairs, *i.e.* couples of SAR images whose interferometric phase is useful for DEM generation (using InSAR techniques) or deformation monitoring, the images have to share almost the same image geometry.

The simple fact that two images are not acquired exactly from the same point in space engenders a loss of coherence, which is called geometric decorrelation (Gatelli *et al.*, 1994). For each SAR system there is a critical perpendicular baseline (the component of the vector that connects the two satellite positions during image acquisition, measured in the direction perpendicular to the SAR (line of sight) which corresponds to a complete deccorrelation of the interferometric phase. For instance, for ERS the critical baseline is about 1100 m: the employed baseline lengths are usually shorter, say of some hundreds of meters. Besides, the constraint on the baseline plays a key role for all DInSAR applications. In Figure 3.6, the geometry of DInSAR is shown.

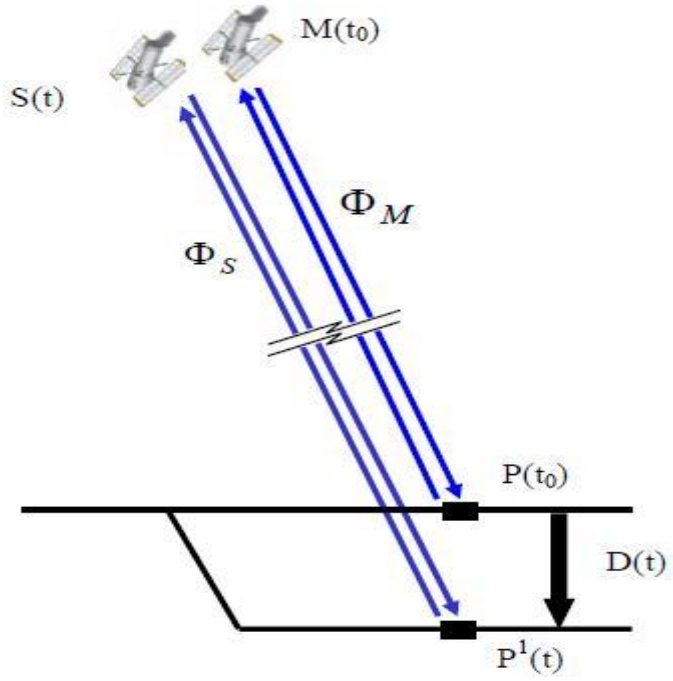

Figure 3.6. DInSAR (Keydel, 2006).

In the following, the principle of the DInSAR technique is briefly summarized.

- The sensors acquire a first SAR image at the time t_0, measuring the phase Φ_M. The first satellite and the corresponding image are usually referred as the master, M.
- Assuming that a land deformation D (t) occurs, which has a given evolution in time, the point P moves to P^1.
- The sensors acquire a second SAR image at the time t, measuring the phase Φ_S. The second satellite is usually referred as the slave, S.

The InSAR techniques exploit the phase difference of Φ_S and Φ_M, named interferometric phase $\Delta\Phi_{Int}$. Assuming that D (t) is naught, *i.e.* the terrain is stable and P' coincides with P, this phase is related to the distance difference SP −MP, which is the key element for the InSAR DEM generation. When the point moves from P to P^1 between two image acquisitions, besides the topographic phase component Φ_{Topo}, $\Delta\Phi_{Int}$ includes the terrain movement contribution, Φ_{Mov}. In the general case $\Delta\Phi_{Int}$ includes:

$$\Delta\varphi_{D\text{-}Int}=\Delta\Phi_{Int}-\Phi_{Topo}-S_{im}=\Phi_{Mov}+\Phi_{Atm}+\Phi_{Res\_Topo}+\Phi_{Noise} \quad (3.3)$$

where Φ_{Topo_Sim} is the simulated topographic component, and Φ_{Res_Topo} represents the residual component due to errors in the simulation of Φ_{Topo}, *e.g.* errors in the employed DEM. In order to derive information on the terrain movement, Φ_{Mov} has to be separated from the other phase components. The techniques that use an external DEM in order to derive the topographic phase component use the so-called two-pass DInSAR configuration. There is another configuration, the three-pass interferometry, which can work without an a priori known DEM, but which requires at least three images acquired over the same scene (Zebker *et al.*, 1994).

There are several factors making the differential interferometry technique a useful tool for either local and regional deformation or change monitoring.

- DInSAR is sensitive to small terrain deformations, up to a few millimeters under optimal measurement conditions, or the centimeter level in general.
- DInSAR provides large area coverage (for example, 100 by 100 km) with a relatively high spatial sampling density (for example, 20 m pixel). To put this in perspective, change at the mm level is being quantified over areas of hundreds of kilometers; this represents a width to accuracy ratio of 10 to the 8th power.
- The increasing availability of long time-series of SAR images (beginning with the ERS satellite sensors in 1991).

3.3. Factors Influencing InSAR Measurements

The phases of images with a difference of position (*e.g.*, two antenna on a plane acquire images simultaneously) or with a difference of time (*e.g.*, one antenna acquires images at two distinct times) can be compared after proper image registration. The resulting difference of phases is a new kind of image called an interferogram (Massonet and Feigl, 1998). Some adverse effects specify the quality of InSAR data which are listed below.

3.3.1. Orbits

A radar interferometer is realized by two antennas that illuminate the same target on the ground surface from two different points. The spatial separation between the antennas leads to shift in the phases coming from the same targets. The phase difference can be calculated if the parallel component of baseline is known. Therefore, precise knowledge of orbits is necessary. If the orbits are not determined precisely and the image shift due to baseline separation is more than half a wavelength per pixel, hundreds of orbital fringes will occur and thus no interferometric effect will be seen (Çakır, 2003).

3.3.2. Temporal Deccorelation

Probably the most important limiting factor in the application of InSAR is temporal decorrelation of the ground between the interferometric acquisitions, and hence losses of meaningful phase relation between corresponding pixels in an image pair. Temporal decorrelation usually results from changes in the complex reflection coefficient of the imaged surface. Changes in the reflection coefficient are generally due to variation in the moisture content or the vegetation. Thus, decorrelation times can be as long as months to years for arid terrain and as short as several hours to several days for rainy and / or forested areas.

Temporal changes in the physical properties of the targets in the scene lead to changes in the reflectivity characteristics of the targets. This, in turn, gives rise to decorrelation between the phases of the two images. Decorrelation or so called ”incoherence” demolishes the quality of the interferograms, leading to random phase changes in each pixel in a given area where fringes are destroyed (Çakır, 2003).

It is important to say that deccorrelation can be appeared for a long time. If the dates can be choose in the same season, temporal deccorrelation can hold in the minimum level.

3.3.3. Baseline Deccorrelation

There is a critical baseline length, above which interferometry becomes impossible. Decorrelation increases with increasing baseline. Because, the baseline determines the topographic sensitivity and hence the altitude of ambiguity of an interferogram, choosing good baselines depends on the applications (Çakır, 2003).

The variation in phase due to baseline is beyond the simple distance and phase relationship that is the basis of DEM and deformation measurements. The variation of phase with viewing geometry leads to a maximum separation between two observation locations that can be used for InSAR analysis. This maximum separation is called the critical baseline, and is dependent on the radar wavelength, the sensor-target distance, the range resolution and the incidence angle.

3.3.4. Topography

Radar observes the topography from two different viewpoints, thus it brings a fundamental stereoscopic effect to light by eliminating a significant fraction of orbital effects. This topographic influence results with some elements that simulate the shape of topography such as contour lines and interference of light waves (Canaslan, 2010).

İnterferometry in areas with strong topography is very good for precise image registration, but steep slopes also lead to deccorrelation. Therefore, if possible, regions with smooth topography should be chosen, minimizes the possibility of the presence of atmospheric artifacts correlated with topography (Çakır, 2003).

3.3.5. Atmospheric Impacts

Atmospheric impact is another significant factor that affects the face of interferogram. If the atmosphere is stable temporally and homogeneous spatially, additional phase delay due to atmospheric conditions would be constant during entire interferometric experience. However, it is difficult to experience this situation practically

and it limits the researches about surface deformation. Atmosphere phase could form very divergent shapes. A study about Etna Volcano reported atmospheric delays about 6±3 cm (Delacourt *et al.*, 1998).

Given sufficient coherence, heterogeneities can often be recognized on the interferogram. Alternatively, the variation due to atmospheric effects can be isolated from multiple interferograms. This is also the approach in using interferometric stacks and in permanent scatterers analysis. In particular, for large numbers of interferograms, the atmospheric effects can be identified as a random process over time and thereby separated from other contributions to the interferometric phase.

4. DATA AND METHODS

4.1. Data Selection

In this study, satellite radar images obtained by Envisat Satellites of ESA are used. Image selection has a great importance in order to conclude the study successfully.

In order to select images, coordinates of research region, track numbers and frame numbers corresponding to those coordinates, whether or not previous radar images of the target region are present and if any the dates and orbital of radar images should be listed.

Data selection and acquisition is the most significant step, as it also influences the subsequent steps. In data selection, the baseline value leads among the most important elements. Image pairs have been formed from the data, based on the baseline values. In data selection, the baseline value (shown in Table 4.1) and image acquisition data between two images are the most significant issues. The length of baseline should be as small as possible in the studies aimed to determine crustal deformation. A glance to topography from two different points would cause a stereoscopic effect due to height. Sensitivity of topography on interferogram is determined with vertical base value. Uncertainty value of height known as altitude of ambiguity (ha) is the height value would cause a fringe. This value indicates that, each height ha would end up with a fringe on interferogram. These are called as “Topographic fringes”.

Table 4.1. Baseline values.

IMAGES		BASELINE	PROGRAM	LEVEL
20060702	20050123	359	ERDAS	1,1
20061015	20050123	201	ERDAS	1,1
20061015	20071104	290	ERDAS	1,1
20061015	20081019	277	ERDAS	1,1
20050309	20050413	351	GMTSAR	1,0

Image selection is obtained by taking sensor type, data compliance, temporal and spatial base distribution and atmospheric characteristics while imaging into account. Sensor and platform characteristics involve some important parameters such as wavelength, SNR (Signal Noise Ratio), orbital slope and repetition period. Accordingly, sensitivity of signals to weather conditions would affect interference density of interferogram caused by topography and deformation (Şengün, 2009).

If we choose DEM in order to remove phase effects, appropriate ha value must be determined with respect to resolution of DEM (Akoğlu, 2001).

Lower vertical base value will lead to directly proportional lower amount of topographic fringes and consequently errors expected to arise due to digital terrain model would be proportionally less. Images could be ordered in either processed form (SLC) or unprocessed, raw form. Advantages of ordering raw images are: a cheapest way provides more control opportunity to the user about phase and ability of re-process the data. The only disadvantage it has, the user spends more time in order to process data but that has ceased to be a problem with today's computer technology.

After data selection, in order to create an interferogram, Gmtsar and Erdas programs are used. For the Gmtsar, C and Fortran programming languages are called in order to form an interferogram with perl scripts. Because of raw images contains data displayed by RAR, the images from SAR should be considered primarily. Thus, focused SLC images could be obtained from each of raw images.

4.2. Digital Elevation Model (DEM)

Shuttle Radar Topography Mission (SRTM) data is used as input of digital elevation data. This is a joint project between SRTM, National Imaging and Mapping Agency (NIMA) and National Aeronautics and Space Administration (NASA). The aim of this project is to generate a DEM of 80 percentage of Earth Surface (The whole area latitudes and longitudes 600N and 500S).Each of the data is established in a second in latitude and longitude terms (Approximately, 30 m). Those data collected in one second interval are called as SRTM1 and it is not publicly available. SRTM3 corresponds to longitude data collected in three seconds interval and it could be easily downloaded from internet.

Height data are all in meter terms and are calculated with respect to EGM96 geoids and WGS84 datum. Horizontal data as geographic coordinates are defined with respect to WGS84 ellipsoid. Data of three seconds consists of rows and columns of 1201x1201. Data format has 16- BIT integer form (Şengün, 2009).

In order to obtain DEM, Stereo SAR model of Radar Module software of Erdas Imagine is used. The purpose of establishment of project file is to record overall process of the experiment step by step. This has importance to avoid data loss in case of any unfavorable condition.

After the establishment of project file, generating interferogram that contains 9 steps of application appears on computer screen. After completion of all those application steps, DEM would be obtained as final product. The model in accordance with boundary coordinates is determined by following DEM formation segment which is already located on its own page. The resulting DEM has 75 m resolution. In other words, edge size of each pixel that forms DEM image corresponds to 75 m in terrain. This issue is known as “pixel size” as well.

4.3. Data Processing

Image selection is the one of the most important decisions in applications of radar interferometry. Image selection involves plenty of criterions such as presence of radar images in demand, orbital information and dates in order to obtain a useful interferogram.

Image selection is obtained by taking sensor type, data compliance, temporal and spatial base distribution and atmospheric characteristics while imaging into account. Sensor and platform characteristics involve some important parameters such as wavelength, SNR (Signal Noise Ratio), orbital slope and repetition period. Accordingly, Sensitivity of signals to weather conditions would affect interference density of interferogram caused by topography and deformation (Şengün, 2009).

The final point to be considered on data processing is unexpected atmospheric impacts. Atmospheric conditions could be acquired by satellite images or ground-based meteorological data (Hanssen, 2001).

The images used for this study are obtained from Envisat satellites. It is required track and frame numbers of the satellite for satellite images involving a segment of studied region. In order to form an interferogram in demand, sufficient number of (at least 10) image must be provided. After listing current images involving application field, images to be match each other should be selected according to their seasonal properties. The most important point to be considered while selecting images is the transition distance between two satellites in the orbital which images are taken. This distance is called as baseline. A glance to topography from two different points would cause a stereoscopic effect due to height. Sensitivity of topography on interferogram is determined with vertical base value.

Uncertainty value of height known as altitude of ambiguity (ha) is the height value would cause a fringe. This value indicates that, each height ha would end up with a fringe on interferogram. These are called as “Topographic fringes“. Altitude of ambiguity parameter is used in order to resolve this (Massonet and Feigl, 1998).

If there is a distant “r“ between two orbital’s, altitude of ambiguity could be calculated like that;

$$h_a=R_s\lambda\tan\Theta m/2r \quad (4.1)$$

In the formula, “Rs” indicates viewpoint range from the target on the surface to second repetition satellite, “Θm” indicates the viewpoint of reference image and “λ” indicates wavelength. Taking 780 km height, 5.66 wavelength and 23° viewpoint of ESR satellites into account, ha~= 10000/d means a topographic fringe will be formed every hundred meters for a vertical 100 meter base.

This factor which is often used in DEM should be removed from the interferogram in case of deformation analysis studies. If DEM is chosen in order to remove the phase effect, appropriate ha value to be used should be determined with respect to resolution of DEM (Akoğlu, 2001).

The lower amount of vertical base indicates lower amount of fringe exactly. As a result of this, errors to be arising due to Digital Terrain Model are expected to be lower in the same amount.

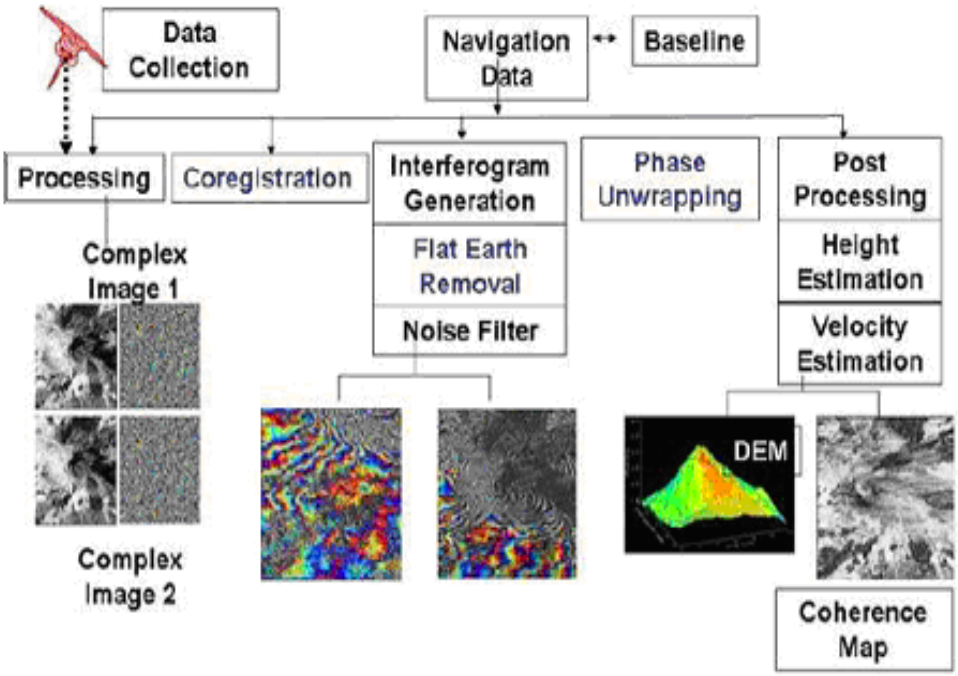

Figure 4.1. Steps of processing (taken from Gmtsar)

In Figure 4.1, creating interferogram steps for the raw data are explained briefly. The first step is processing including focusing step. After focusing raw images in order to form an interferogram, two images must be corrected and aligned to avoid pixel shifts in their positions depending upon their geometry or any other possible conditions. The program calculates the errors such as shift, tension by utilizing amplitude values of two complex images in order to align the images precisely. If the shift value is significantly major, error value must be calculated manually. Images are re-sampled after the determination of shift value.

After the alignment of images relatively to each other, the complex pixel phase component of each of reference image is removed from the correspondent complex pixel phase component of the other image. Phase values of complex image forms our interferogram. Phase values are multiples of 2π. Once the interferogram is formed, it could be filtered if desired (Goldstein and Werner, 1998). After filtering, it is possible to give a start to “unwrap“ process. Geocode correction is put as a final step. This process facilitates the cooperation of interferogram with other earth science data. The interferogram oriented

in viewpoint of radar through the entire process fit in geographical coordinates. Figure 4.2 shows the pictures that created by the help of Erdas Imagine.

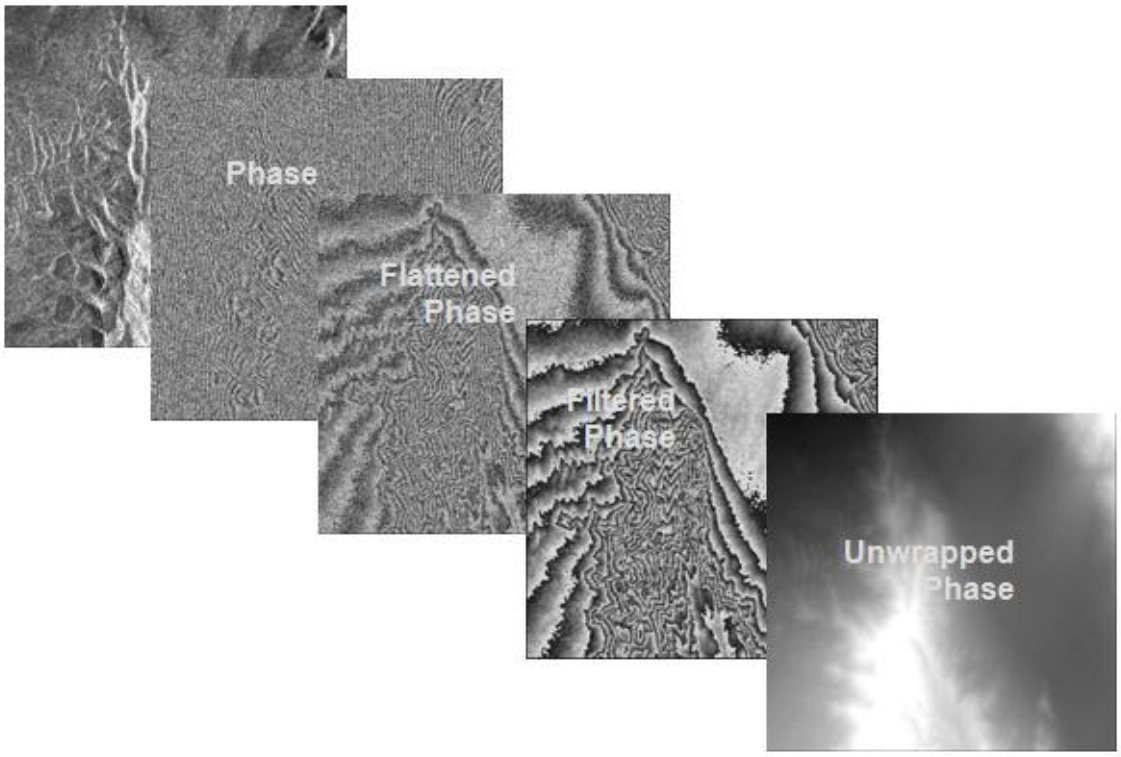

Figure 4.2. Steps of the interferograms (taken from Erdas Imagine).

Each of fringes appears blue to blue in the interferogram indicates 2.8 displacement between the ground towards line of sight and the radar. As level 0 and level 1 images of the region are present, the process is continued with two programs. Level 0 data were evaluated with Gmtsar written in Fortran language and Level 1 data were evaluated with Erdas Imagine program. In order to create interfrogram; in every steps, different scientific programs were used. These programs are displayed in Figure 4.3.

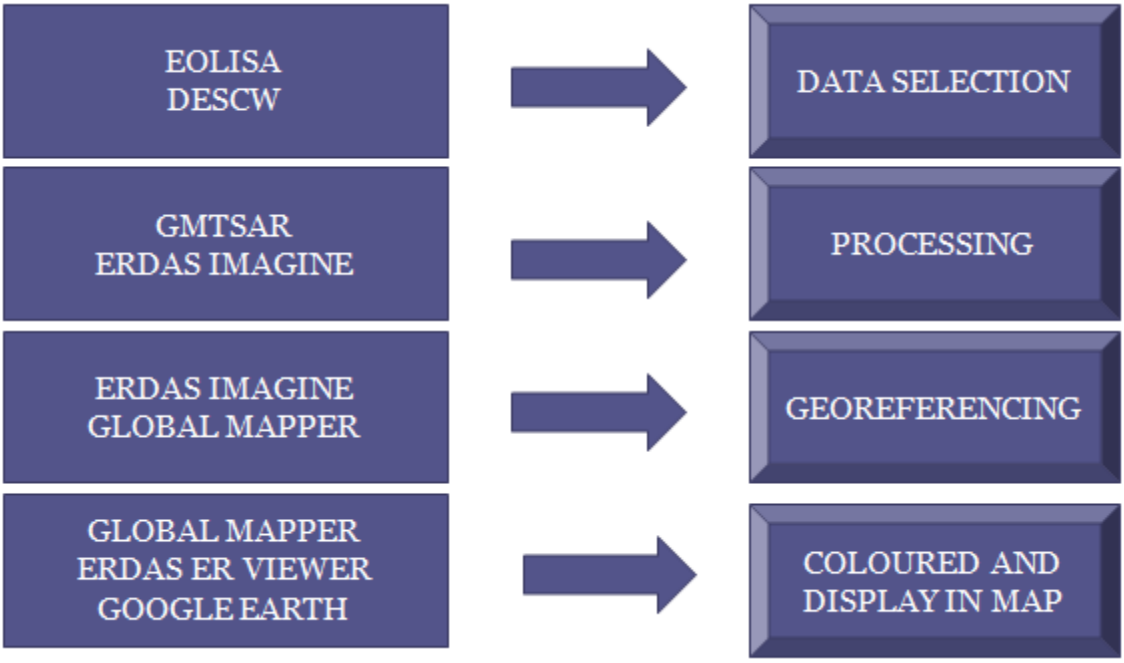

Figure 4.3. Programs.

5. RESULTS

Seven different images were used to generate five interferogram which are shown in Figure 5.1, Figure 5.2, Figure 5.3, Figure 5.4 and Figure 5.5. Every fringe in the interferogram refers to a displacement about 2.8 cm corresponding to a half wave length according to line of sight.

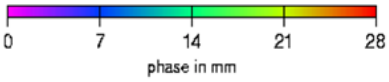

20060702-20050123

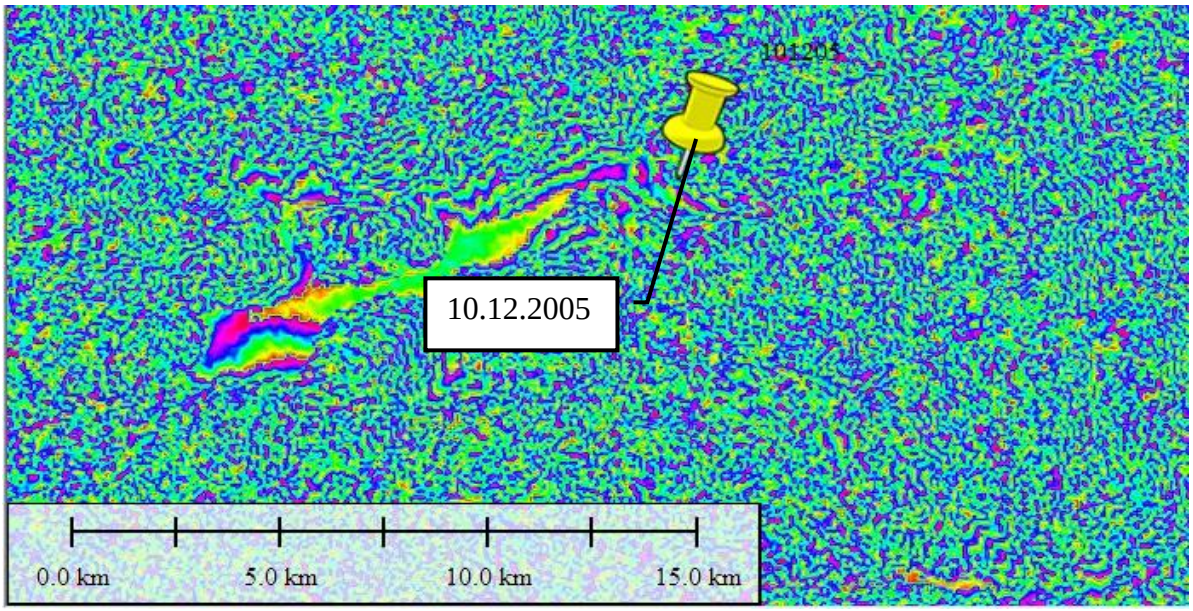

Figure 5.1. First interferogram.

20061015-20050123

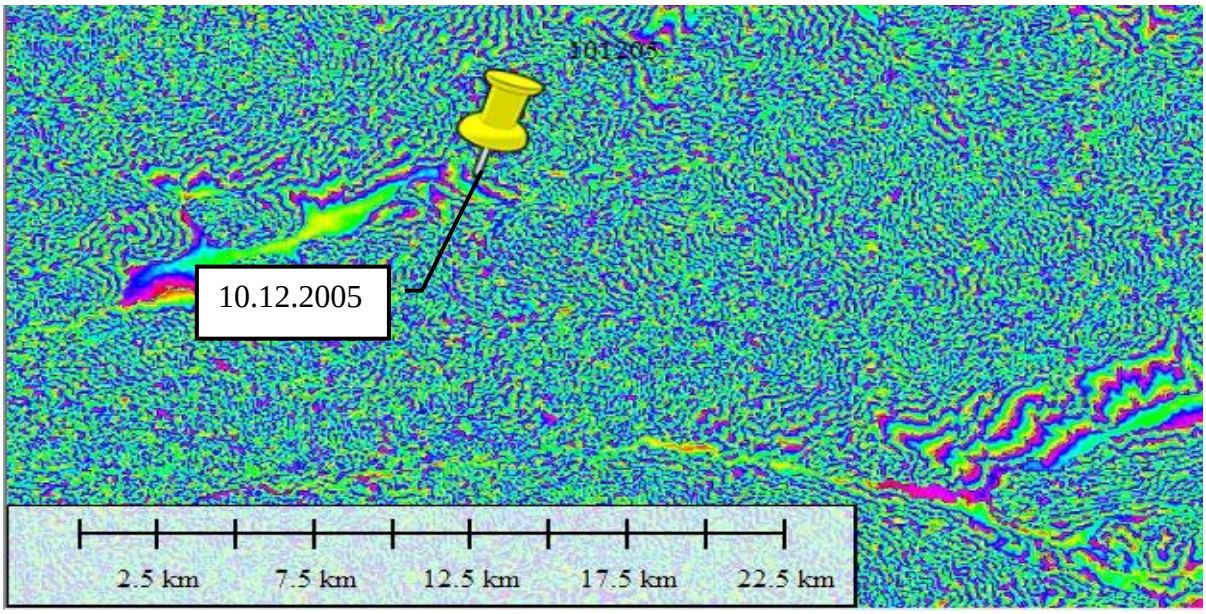

Figure 5.2. Second interferogram.

20061015-20071104

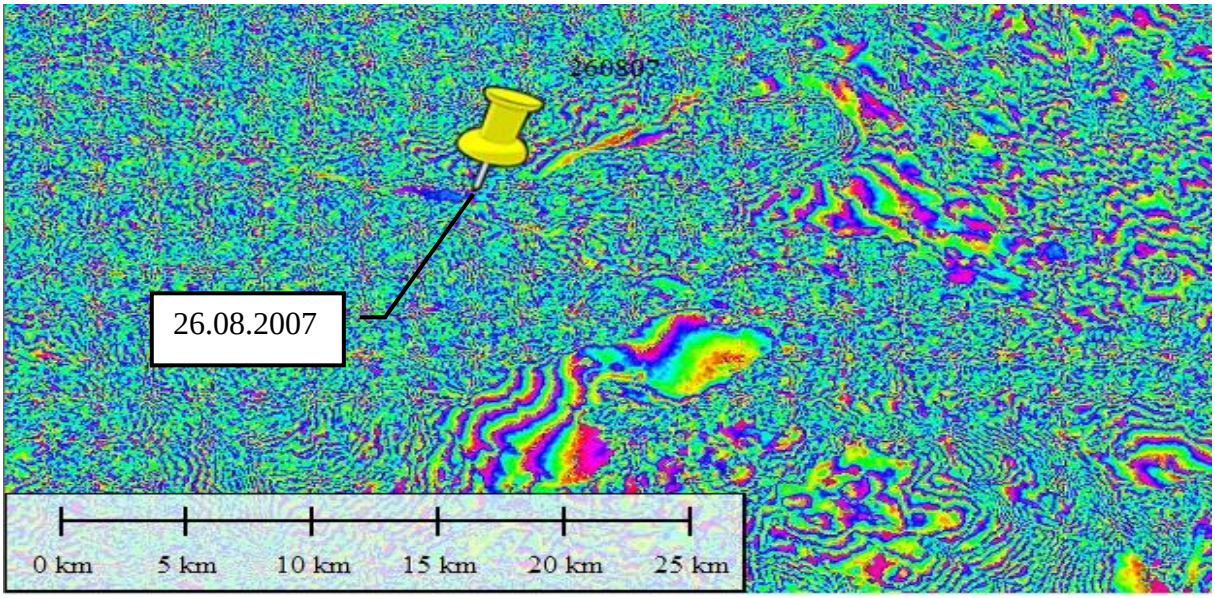

Figure 5.3. Third interferogram.

20061015-20081019

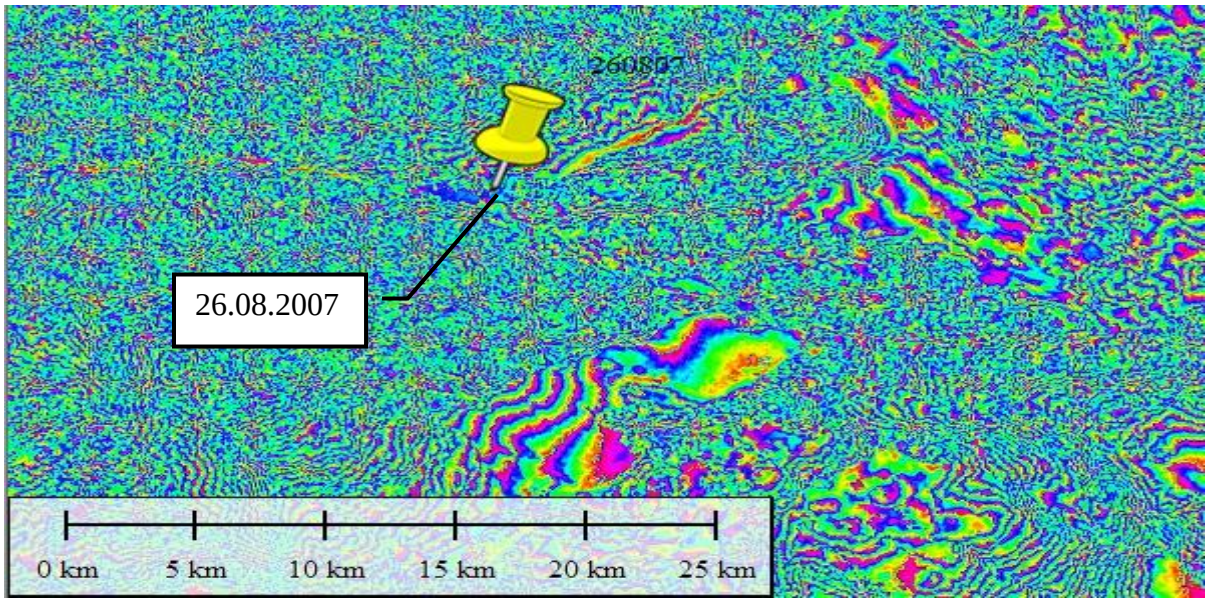

Figure 5.4. Fourth interferogram.

20050309-20050413

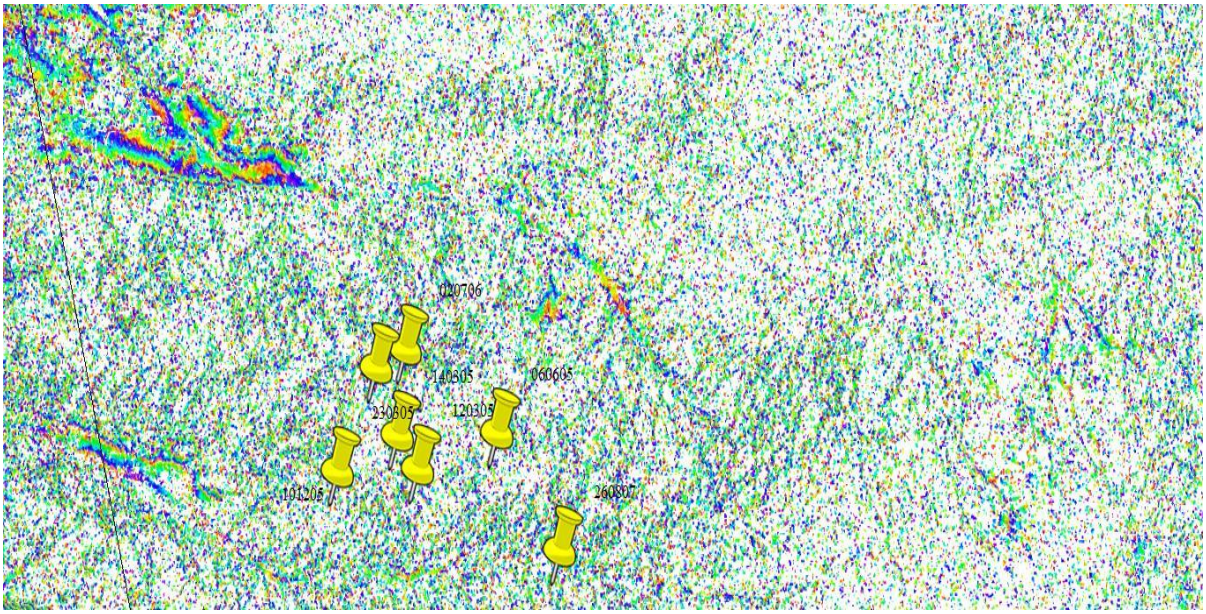

Figure 5.5. Noisy interferogram.

6. DISCUSSION

In the study area, the deformations resulting from moderate earthquakes that occurred during 2005-2006-2007 have been examined. Radar images that shown in Table 6.1, have been provided by the ESA.

Table 6.1. List of images.

IMAGES
ASA_IMS_1PNUPA20050123_190041_000000162034_00085_15169_6857
ASA_IMS_1PNUPA20060702_190043_000000162049_00085_22684_6859
ASA_IMS_1PNUPA20081019_190032_000000162073_00085_34708_6858
ASA_IMS_1PNDPA20061015_190042_000000162052_00085_24187_1024
ASA_IMS_1PNDPA20071104_190034_000000162063_00085_29698_1025
ASA_IM__0CNPDK20050309_073031_000000172035_00221_15806_0102
ASA_IM__0CNPDK20050413_073036_000000162036_00221_16307_1085

Within the scope of the study, images have been assessed using the open source-code Gmtsar and Erdas Imagine programs. For the map display, the Global Mapper software has been used. The Global Mapper software has allowed us to display the interferogram and the files with .kmz extension collectively, specifying location of earthquakes.

In InSAR, image processing consists of three steps in general:

- Data Selection
- Data Processing
- Verification

Data selection and acquisition is the most significant step, as it also influences the subsequent steps. In data selection, the baseline value leads among the most important elements. Image pairs have been formed from the data, based on the baseline values. In data selection, the baseline length and image acquisition date between two images are the most significant issues. The length of baseline should be as small as possible in the studies

aimed to determine crustal deformation. Some of these image pairs have proven to be meaningful, while some have been meaningless.

- Within the scope of the thesis, it has been attempted to determine the deformations that have emerged following the 10.12.2005 and 26.08.2007 Karlıova Earthquakes with the InSAR technique. The earthquakes experienced in the area between the years 2005 and 2007 have been listed in Table 6.2.

Table 6.2. Earthquakes.

Date	**Lat (N°)**	**Lon(N°)**	**Dept. (km.)**	**Magnitude**
12.03.2005	39.39	40.85	8	5.4
12.03.2005	39.39	40.90	16	4.2
14.03.2005	39.35	40.87	10	5.9
14.03.2005	39.40	40.82	14	4.9
15.03.2005	39.41	40.83	8	4.2
18.03.2005	39.37	40.87	6	4.2
18.03.2005	39.41	40.76	12	4.0
23.03.2005	39.37	40.81	10	5.4
23.03.2005	39.39	40.79	10	4.9
25.03.2015	39.43	40.72	4	3.9
02.04.2005	39.39	40.83	4	4.0
06.06.2005	39.37	40.93	8	5.7
10.08.2005	39.35	41.09	6	4.3
10.12.2005	**39.38**	**40.86**	**18**	**5.2**
02.07.2006	39.31	40.94	6	4.9
21.07.2006	39.37	40.82	4	4.1
26.08.2007	**39.26**	**41.04**	**5**	**5.1**

- Looking at the particulars of the area, it is observed that earthquakes of magnitude four and above are frequently experienced, while there are four earthquakes of magnitude over five during the years 2005-2007.

- With the images obtained from the Envisat satellite, the 10.12.2005 and 26.08.2007 earthquakes at Karlıova have been examined and interferograms

have been generated. The images, baseline values, the used program and image level data that have been selected for the generated interferograms have been provided in Table 6.3.

Table 6.3. Property of images.

IMAGES		BASELINE	USED PROGRAM	LEVEL
20060702	20050123	359	ERDAS	1,1
20061015	20050123	201	ERDAS	1,1
20061015	20071104	290	ERDAS	1,1
20061015	20081019	277	ERDAS	1,1
20050309	20050413	351	GMTSAR	1,0

- For the 10.12.2005 earthquake, radar images dated 20050123 and 20060702 have been taken and a deformation of two fringes has been determined. The same result has been obtained with another interferogram for the same earthquake that has been generated by the data dated 20050123 and 20061015.

- Meanwhile, for the earthquake dated 26.08.2007, radar images dated 20061015 and 20071104 have been taken and a deformation by five fringes has been determined. In the interferogram generated by the data dated 20061015 and 20081019, the same conclusion has been reached.

- As it is well known, McClusky *et al*. (2000) present GPS measurements of crustal motion between 1988-1997 for Mediterranean and Caucasus. Their study gives a slip rate of 24±1 mm/yr for NAF. They stated that eastern Turkey is characterized by distributed deformation. Reilinger *et al*. (2006) also present GPS derived velocity field for the period 1988-2005 in the Africa-Arabia-Eurasia continental collision zone. Their results indicate that counterclockwise rotation of Turkey relative to Eurasia varies in the range of 20-30 mm/yr. A recent work by Aktuğ *et al.* (2012) obtained a maximum slip rate of 13 mm/yr in

the study area on the EAFS branch decreasing to 7.5 mm/yr in the north of the Karlıova Triple Junction.

- The time range of the radar images that have been acquired for the earthquakes examined within the scope of the thesis is 2005-2008. The velocity values (relative to Eurasia in ITRF 2005 reference frame) obtained from the episodic GPS measurements made at the area during 2003-2005 by Özener *et al*. (2010), vary in the range of 16-24 mm/year. Again, the velocity (relative to Eurasia in ITRF2005 reference frame) obtained from the data during 2009-2012, of the CORS-TR stations (BING, ERZI and TNCE) that are available in the research area and established in 2008, reaches up to maximum 20 mm/year. The displacement vectors at the GPS values are three dimensional. The displacement amounts obtained from InSAR are single-dimensional in line of sight view. In order to be able to compare two different groups of measurements, it is necessary to project the GPS displacement vectors in the line of sight. To that end, the GPS vectors have been projected onto the satellite view direction, using the following formula. GPS measurements are projected to the LOS vector as follows:

$$GPS_{los}=GPS_{north} \text{ x } (-1) * \cos(\gamma-(3\pi/2) * \sin(\Theta) + GPS_{east} * (-1)$$

$$* \sin(\gamma-(3\pi/2) * \sin(\Theta) + GPS_{up} * \sin(\Theta) \quad (4.2)$$

Where "γ" indicates the satellite's orbit angle relative to true north and "Θ" indicates the incidence angle of the radar wave (Hanssen, 2001). GPS_{north} is the north component; GPS_{east} is the east component of the velocity.

- In line with the above formula, the velocity of the episodic GPS stations, available in the area, in the line of sight has been calculated to be approximately four mm during 2003-2005; and the speed value of the continuous GPS stations in the line of sight has been calculated as approximately five mm during 2009-2012.

- With this study using the InSAR technique, for two separate earthquakes (10.12.2005 Mw=5.2 Depth:18 km and 26.08.2007 Mw=5.1 Depth:5,0 km), a deformation in the line of sight of 56 mm during 2005-2006 and 140 mm during 2006-2008 has been determined respectively. In the interferograms generated by using the radar images in the C-band, one fringe theoretically corresponds to a deformation of half the radar wavelength. Therefore, deformations less than 28 mm in the area cannot be determined by the InSAR technique. The SAR data differ from the GPS data in time. During this time range, 17 earthquakes of moderate magnitude have also occurred in the area. The results differ from each other significantly since InSAR measurements contain post-seismic deformation while GPS observations do not. The spatial density of GPS sites is limited. Moreover, noisy interferograms due to atmospheric signal, and phase unwrapping errors affects the accuracy assessment and interpretation of the results.

REFERENCES

Aksoy E, M. İnceöz, A. Koçyiğit, 2007, "Lake Hazar basin: A Negative Flower Structure on the East Anatolian Fault System (EAFS)*", Turkish J. Earth Sci.* Vol.16, pp. 319-338. Turkey.

Allen, C. R. (1969), "Active Faulting in Northern Turkey", *Div. of Geol. Sic., Calif. Inst. of Technol*, Vol. 1577, pp. 32, Pasadena.

Akabalı, O. A.,*2002, Stereo Yapay Açıklıklı Radar Görüntülerinden Otomatik Sayısal Yükseklik Modeli Üretilmesi ve Doğruluğunun Araştırılması*,M.S. Thesis, YTU, İstanbul.

Aklıouat, H., Y. Smara, L. Bouchemakh, 2007, *"*Syhentetic Aperture Radar Image Formation Process:Application to aRegion of North Algeria*"*, Montreuz, Switzerland, 23-27 April 2007, Vol.636, Faculty of Electronics and Computer Sciences.University of Sciences and Technology Houari Boumediene.

Akoğlu, A. M., 2001, *17 Ağustos 1999 İzmit Depremi Postsismik Deformasyonlarının Sentetik Açıklık Radar İnterferometrisi Yöntemi ile İncelenmesi*, MS Thesis, İ.T.Ü. Avrasya Yer Bilimleri Enstitüsü, İstanbul.

Aktuğ, B., U. Dikmen, A. Doğru, H. Özener, 2013. "Seismicity and Strain Accumulation around Karlıova Triple Junction", *Journal of Geodynamics*, Volume 67, pp. 21–29.

Arpat, E., and F. Şaroğlu (1972), "Some Observations and Thoughts on the East Anatolian Fault", Bull. Miner. Res. Explor. Inst. Turk., Vol.73, pp. 44–50.

ASF, 2002, *Alaska Satellite Facility: University of Alaska*, http://www.asf.alaska.edu/~rgens/teaching/asf_seminar/2002/

Ausherman, A., Kozma, J. Walker., H. Jones and E. Poggio,1984, "Developement in Radar Imaging", Vol. 20, pp. 363-400.

Canaslan, F., 2010, *İnsar Yöntemiyle Düşey Yönlü Yüzey Deformasyonlarının Belirlenmesi, Konya Örneği*, M.S. Thesis, Selçuk University, İstanbul

Çakır, Z., 2003, *Analysis Of The Crustal Deformation Caused By The 1999 İzmit and Düzce Earthquakes Using Synthetic Aperture Radar Interferometry*, PhD Thesis, ITU Geological Engineering, Istanbul, Turkey.

Çakır, Z., J. B. Chabalier, R. Armijo, B. Meyer, A. Barka and G. Peltzer, 2003, "Coseismic and Early Post-Seismic Slip Associated with the 1999 İzmit Earthquake (Turkey), From SAR Interferometry and Tectonic Field Observations", *Geophysical Journal International*, Vol.155, No. 1, pp. 93-110.

Çetin, F.,2010, *1 Ekim Dinar Depremi Faylanma Parametrelerinin İnsar ve Sismoloji Verileriyle Belirlenmesi*, M.S. Thesis,

CCRS, 2013, *Canada Centre for Remote Sensing: Technique of InSAR* http://www.nrcan.gc.ca/earth-sciences/about/organization/organization structure/ Canada-centre-for-remote-sensing /11740

Curlander, J. C. and R. N. McDonough, 1991," Synthetic Aperture Radar: Systems and Signal Processing", *John Wiley*, pp. 647, New York.

L. Cutrona, E. Leith, L. Porcello and W. Vivian, 1966, "On the Application of Coherent Optical Processing Techniques to Synthetic Aperture Radar", *Proceeding of the IEEE*, Vol. 54, pp.1026-1032,

Delacourt, C., P. Briole and J. Achache, 1998, "Tropospheric Corrections of SAR Interferograms with Strong Topography. Application to Etna", *Geophysical Research Letters*, Vol.25, pp. 2849-2852.

Dilia, R., Domingo, R., 1999, "A SAR Algorithm Development Environment Using Matlab*"*, CRC-99, *Computing Research Conference,* Mayaguez Puerto Rico.

Elachi, C. 1987 *"*Introduction to the Physics and Techniques of Remote Sensing*", John Wiley*, New York, pp. 413

Emre Ö., S. Özalp, C. Yıldırım, V. Özaksoy, A. Doğan, 2005, *Evaluation of March 12 and 14, 2005 Karlıova Earthquakes.*, MTA. Report.

ESA, 2013, *European Space Agency: What is Envisat*, https://earth.esa.int/web/guest/missions/esa-operational-eo-missions/envisat

Gabriel, A. K., R. M. Goldstein and H. A. Zebker, 1989, "Mapping Small Elevation Changes over Large Areas: Differential Radar Interferometry", *Journal of Geophysical Research*, Vol. 94, pp. 9183-9191.

Gatelli F, A. Monti, A. Guarnieri, F. Parizzi, P. Pasquali, C. Prati and F. Rocca, 1994, "The Wavenumber Shift in SAR Interferometry", *IEEE Trans. Geosci. Remote Sens*. Vol. 32, pp. 855–65

GMTSAR, 2013, *GMT* Synthetic *Aperture Radar: Steps of InSAR*, http://topex.ucsd.edu/gmtsar/tar/GMTSAR.pdf

Goldstein, R. M. and C. L. Werner, 1998, "Radar Interferogram Filtering for Geophysical Applications", *Geophysical Research Letters*, Vol. 25, pp. 4035-4038.

Graham, L. C., 1974, "Synthetic Interferometer Radar for Topographic Mapping", *Proceedings of the IEEE*, Vol. 62, pp. 763-768.

Gülkan, P., A. Koçyiğit, M. S. Yücemen, V. Doyuran and N. Başöz, 1993, *En Son Verilere Göre Hazırlanan Türkiye Deprem Bölgeleri Haritası*, ODTÜ, Report No. 93-01.

Hanssen, R. F., 2001, *Radar Interferometry: Data Interpretation and Error Analysis*, Kluwer Academic Publishers, Dordrecht.

Hempton, M. R., J. F. Dewey, and F. Şaroğlu, 1981, "The East Anatolian Transform Fault: Along strike variations in geometry and behaviour", *Eos Trans*. AGU, vol. 62, pp. 393.

Karimzadeh, S, F. F. Ahmedi,2013,"Using Advanced Space-borne Radar Technology for Detection and Measurement of Land Subsidence and Interseismic Slip Rates, the Case Study: NW Iran", *Studies in Surveying and Mapping Science (SSMS),*Vol. 1, No.1,pp. 1-9, March.

Köse, M. H.2006, *Uydu Radar Görüntülerinden Üç Boyutlu Sayısal Arazi Modelin Üretilmesi,* M.S. Thesis, Selçuk University, Science Institute, Konya.

Lyons, S. and D. Sandwell, 2002, "Fault Creep along the Southern San Andreas from InSAR, Permanent Scatterers, and Stacking", *Journal of Geophysical Research*, Vol.108, pp. 24

MacDonald, H. C., 1969, *Geologic Evaluation of Radar Imagery from Eastern Panama and Northwestern Colombia,* Ph.D. Dissertation, Kansas.

Massonnet, D. and K. L. Feigl, 1998, "Radar Interferometry and Its Application to Changes in the Earth's Surface", *Reviews of Geophysics*, Vol.36, pp. 441-500.

Massonnet, D., M. Rossi., C. Carmona, F. Adagna, G. Peltzer, K. Feigl and T. Rabaute, 1993, "The Displacement Field of the Landers Earthquake Mapped by Radar Interferometry", *Nature*, Vol. 364, pp. 138-142.

McClusky, S., S. Balassanian, A. Barka, C. Demir, S. Ergintav, I. Georgiev, O. Gürkan, M. Hamburger, K. Hurst, H. Kahle, K. Kastens, G. Kekelidze, R. King, V. Kotzev, O. Lenk, S. Mahmoud, A. Mishin, M. Nadariya, A. Ouzounis, D. Paradissis, Y. Peter,

M. Prilepin, R. Reilinger, I. Şanlı, H. Seeger, A. Tealeb, M. N . Toksöz, G. Veis, 2000, "Global Positioning System Constraints on Plate Kinematics and Dynamics in the Eastern Mediterranean and Caucasus", *J. Geophys. Res*. Vol. 105, pp. 5695-5719.

McKenzie, D., 1972, " Active Tectonics of The Mediterranean Region", *Geophys. J. Royal Astron. Soc*, Vol. 30, No.2, pp. 109-185.

Över, S., S. Özden, and H. Yılmaz, 2004, "Late Cenozoic Stress Evolution along the Karasu Valley, SE Turkey", *Tectonophysics*, Vol. 380, ppt. 43–68,

Özener, H., E. Arpat, S. Ergintav, A. Doğru, R. Çakmak, B. Turgut, U. Doğan, 2010, "Kinematics of the eastern part of the North Anatolian Fault Zone", *J. Geodynamics*, Vol. 49, pp. 141-150.

Radar Tutorial, 2013, *Waves and Frequency Rangers*, http://www.radartutorial.eu/07.waves/wa04.en.html

Reilinger, R., S. McClusky, P. Vernant, S. Lawrence, S. Ergintav, R. Çakmak, H. Özener, F. Kadirov, I. Guliev, R. Stepanyan, M. Nadariya, G. Hahubia, S. Mahmoud, K. Sakr, A. Arrajehi, D. Paradissis, A. Al-Aydrus, M. Prilepin, T. Guseva, E. Evren, A. Dmitrotsa, S. V. Filikov, F. Gomez, R. Al-Ghazzi, G. Karam, 2006, "GPS Constraints on Continental Deformation in the Africa–Arabia–Eurasia Continental Collision Zone and Implications for the Dynamics of Plate Interactions." *Journal of Geophysical Research*, Vol. 111.

Rogers, A.E.E. and R.P. Ingalls, 1969, "Venus: Mapping the Surface Reflectivity by Radar Interferometry", *Science*, Vol.165, pp. 797-799.

Rosen, P., S. Hensley, I. R. Joughin, Li, F. K., S. Madsen, E. Rodriguez and R. Goldstein, 2000, " Synthetic Aperture Radar Interferometry", *Proceedings of the IEEE*, Vol.88,pp. 333-382.

Rosen, P., C. Werner, E. Fielding, S. Hensley, S. Buckley and P. Vincent, 1998, "Aseismic Creep Along The San Andreas Fault Northwest of Parkfield, CA Measured by Radar Interferometry", *Geophysical Research Letters*, Vol. 25, pp. 825-828.

Şaroğlu, F., O. Emre, and İ. Kuşçu, 1992, "Active Fault Map of Turkey", *Gen. Dir. Of Miner. Res. and Explorer*., Ankara.

Şengör, A. M. C., *et al.*, 1985, "Strike-slip Faulting and Related Basin Formation in Zones of Tectonic Escape: Turkey as a Case Study, in Strike-Slip Deformation, Basin Formation and Sedimentation" in K. T. Biddle and N. Christie-Blick (eds.), *Spec. Publ. Soc. Econ. Paleontol. Mineral,* Vol. 37, pp. 227–264.

Şengün, Y.S., 2009, *Gps ve İnsar Ölçülerinin Birlikte Kullanarak İzmit Depreminde Oluşan Deformasyonların Belirlenmesi:Nokta Seyrekleştirmede Yeni Bir Algoritma, Ph.D. Dissertation,* İstanbul Technical University.

Şengün, Y.S., Deniz, R., 2009, *İnsar Ölçülerinin Doğruluk Araştırması ve Nokta Seyrekleştirmesi,* Ph.D. Dissertation, İstanbul Technical University.

UN/ISDR, 2013, *The United Nations Office for Disaster Risk Reduction,* http://www.unisdr.org/we/inform/disaster-statistics

Uslu K., 2002, *İnterferometrik SAR Verisi İşlenmesi ve Bir Simülasyon Örneği*, M.S., YTÜ, İstanbul.

Webb, L.H., J. David, J. Munson, J.S.Stacy, 1998, "High Resolution Planetary Imaging Via Spotlight – Mode SAR", *IEEE Transactions on Image Processing*,Vol. 7, No. 11, pp. 1571-1582, November

Westaway, R., 2004, "Kinematic Consistency Between the Dead Sea Fault Zone and the Neogene and Quaternary Left-Lateral Faulting in SE Turkey", *Tectonophysics*, Vol. 391, pp. 203–237,

Wright, T., 2000, *Crustal Deformation in Turkey from Synthetic Aperture Radar Interferometry*, Ph.Dissertation, University of Oxford.

Wright, T. J., B. E. Parsons and Z. Lu, 2001, "Towards Mapping Surface Deformation in Three Dimensions Using InSAR", *Geophysical Research Letters*, Vol. 31, pp. 5.

Yavaşoğlu, H., E. Tarı, 2011, "Anadolu Fayının Orta Bölümündeki Güncel Tektonik Aktivitenin Belirlenmesi" *ITU Journal Series D: Engineering,* Vol. 9, No. 6, pp. 73.

Yılmaz, H., S. Över, and S. Özden, 2006, "Kinematics of the East Anatolian Fault Zone Between Türkoğlu (Kahramanmaraş) and Çelikhan (Adıyaman), Eastern Turkey", *Earth Planets Space*, Vol. 58, pp. 1463–1473

Zebker, H. A., P. A. Rosen, R. M. Goldstein, A. Gabriel and C. L. Werner, 1994, "On The Derivation of Coseismic Displacement Fields Using Differential Radar Interferometry: The Landers Earthquake", *J. Geophys. Res., Vol.* 99, No.19, 617-643.

Zebker, H. A., C. L. Werner, P. A. Rosen, S. Hensley, 1994, " Accuracy of Topographic Maps Derived from ERS-1 Interferometric Radar", *IEEE transactions on Geoscience and Remote Sensing*, Vol.32, pp. 823-836.

Zisk, S. H., 1972, "A New Earth-based Radar Technique for The Measurement of Lunar Topography", *Moon*, Vol.4, pp. 296-306.

Zou, W., Y. Li, Z. Li and X. Ding2009, "Improvement of the Accuracy of InSAR Image Co-registration Based on Tie Points – a review", *Sensors*, Vol. 9, pp. 1259-1281.